

# Spectral Clustering, Bayesian Spanning Forest, and Forest Process

Leo L. Duan\*     Arkaprava Roy †

April 14, 2023

## Abstract

Spectral clustering views the similarity matrix as a weighted graph, and partitions the data by minimizing a graph-cut loss. Since it minimizes the across-cluster similarity, there is no need to model the distribution within each cluster. As a result, one reduces the chance of model misspecification, which is often a risk in mixture model-based clustering. Nevertheless, compared to the latter, spectral clustering has no direct ways of quantifying the clustering uncertainty (such as the assignment probability), or allowing easy model extensions for complicated data applications. To fill this gap, we propose the Bayesian forest model as a generative graphical model for spectral clustering. This is motivated by our discovery that the posterior connecting matrix in a forest model has almost the same leading eigenvectors, as the ones used by normalized spectral clustering. To induce a distribution for the forest, we develop a “forest process” as a graph extension to the urn process, while we carefully characterize the differences in the partition probability. We derive a simple Markov chain Monte Carlo algorithm for posterior estimation, and demonstrate superior performance compared to existing algorithms. We illustrate several model-based extensions useful for data applications, including high-dimensional and multi-view clustering for images.

*Keywords:* Graphical Model Clustering; Model-based Clustering; Normalized Graph-cut; Partition Probability Function.

---

\*Department of Statistics, University of Florida, li.duan@ufl.edu

†Department of Biostatistics, University of Florida, ark007@ufl.edu

# 1 Introduction

Clustering aims to partition data  $y_1, \dots, y_n$  into disjoint groups. There is a large literature ranging from various algorithms such as K-means and DBSCAN (MacQueen, 1967; Ester et al., 1996; Frey and Dueck, 2007) to mixture model-based approaches [reviewed by Fraley and Raftery (2002)]. In the Bayesian community, model-based approaches are especially popular. To roughly summarize the idea, we view each  $y_i$  as generated from a distribution  $\mathcal{K}(\cdot | \theta_i)$ , where  $(\theta_1, \dots, \theta_n)$  are drawn from a discrete distribution  $\sum_{k=1}^K w_k \delta_{\theta_k^*}(\cdot)$ , with  $w_k$  as the probability weight, and  $\delta_{\theta_k^*}$  as a point mass at  $\theta_k^*$ . With prior distributions, we could estimate all the unknown parameters ( $\theta_k^*$ 's,  $w_k$ 's, and  $K$ ) from the posterior.

The model-based clustering has two important advantages. First, it allows important uncertainty quantification such as the probability for cluster assignment  $c_i$ ,  $\Pr(c_i = k | y_i)$ , as a probabilistic estimate that  $y_i$  comes from the  $k$ th cluster ( $c_i = k \Leftrightarrow \theta_i = \theta_k^*$ ). Different from commonly seen asymptotic results in statistical estimation, the clustering uncertainty does not always vanish even as  $n \rightarrow \infty$ . For example, in a two-component Gaussian mixture model with equal covariance, for a point  $y_i$  at nearly equal distances to two cluster centers, we would have both  $\Pr(c_i = 1 | y_i)$  and  $\Pr(c_i = 2 | y_i)$  close to 50% even as  $n \rightarrow \infty$ . For a recent discussion on this topic as well as how to quantify the partition uncertainty, see Wade and Ghahramani (2018) and the references within. Second, the model-based clustering can be easily extended to handle more complicated modeling tasks. Specifically, since there is a probabilistic process associated with the clustering, it is straightforward to modify it to include useful dependency structures. We list a few examples from a rich literature: Ng et al. (2006) used a mixture model with random effects to cluster correlated gene-expression data, Müller and Quintana (2010); Park and Dunson (2010); Ren et al. (2011) allowed the partition to vary according to some covariates, Guha and Baladandayuthapani

(2016) simultaneously clustered the predictors and use them in high-dimensional regression.

On the other hand, model-based clustering has its limitations. Primarily, one needs to carefully specify the density/mass function  $\mathcal{K}$ , otherwise, it will lead to unwanted results and difficult interpretation. For example, Coretto and Hennig (2016) demonstrated the sensitivity of the Gaussian mixture model to non-Gaussian contaminants, Miller and Dunson (2018) and Cai et al. (2021) showed that when the distribution family of  $\mathcal{K}$  is misspecified, the number of clusters would be severely overestimated. It is natural to think of using more flexible parameterization for  $\mathcal{K}$ , in order to mitigate the risk of model misspecification. This has motivated many interesting works, such as modeling  $\mathcal{K}$  via skewed distribution (Frühwirth-Schnatter and Pyne, 2010; Lee and McLachlan, 2016), unimodal distribution (Rodríguez and Walker, 2014), copula (Kosmidis and Karlis, 2016), mixture of mixtures (Malsiner-Walli et al., 2017), among others. Nevertheless, as the flexibility of  $\mathcal{K}$  increases, the modeling and computational burdens also increase dramatically.

In parallel to the above advancements in model-based clustering, spectral clustering has become very popular in machine learning and statistics. Von Luxburg (2007) provided a useful tutorial on the algorithms and a review of recent works. On clustering point estimation, spectral clustering has shown good empirical performance for separating non-Gaussian and/or manifold data, without the need to directly specify the distribution for each cluster. Instead, one calculates a matrix of similarity scores between each pair of data, then uses a simple algorithm to find a partition that approximately minimizes the total loss of similarity scores across clusters (adjusted with respect to cluster sizes). This point estimate is found to be not very sensitive to the choice of similarity score, and empirical solutions have been proposed for tuning the similarity and choosing the number of clusters (Zelnik-Manor and Perona, 2005; Shi et al., 2009). There is a rapidly growing literature of

frequentist methods on further improving the point estimate [Chi et al. (2007); Rohe et al. (2011); Kumar et al. (2011); Lei and Rinaldo (2015); Han et al. (2021); Lei and Lin (2022); among others], although, in this article, we focus on the Bayesian perspective and aim to characterize the probability distribution.

Due to the algorithmic nature, spectral clustering cannot be directly used in model-based extension, or produce uncertainty quantification. This has motivated a large Bayesian literature. There have been several works trying to quantify the uncertainty around the spectral clustering point estimate. For example, since the spectral clustering algorithm can be used to estimate the community memberships in a stochastic block model, one could transform the data into a similarity matrix, then treat it as if generated from a Bayesian stochastic block model (Snijders and Nowicki, 1997; Nowicki and Snijders, 2001; McDaid et al., 2013; Geng et al., 2019). Similarly, one could take the Laplacian matrix (a transform of the similarity used in spectral clustering) or its spectral decomposition, and model it in a probabilistic framework (Socher et al., 2011; Duan et al., 2019).

Broadly speaking, we can view these works as following the recent trend of robust Bayesian methodology, in conditioning the parameter of interest (clustering) on an insufficient statistic (pairwise summary statistics) of the data. See Lewis et al. (2021) for recent discussions. Pertaining to Bayesian robust clustering, one gains model robustness by avoiding putting any parametric assumption on within-cluster distribution  $\mathcal{K}(\cdot | \theta_k^*)$ ; instead, one models the pairwise information that often has an arguably simple distribution. Recent works include the distance-based Pólya urn process (Blei and Frazier, 2011; Socher et al., 2011), Dirichlet process mixture model on Laplacian eigenmaps (Banerjee et al., 2015), Bayesian distance clustering (Duan and Dunson, 2021a), generalized Bayes extension of product partition model (Rigon et al., 2020).

This article follows this trend. Instead of modeling  $y_i$ 's as conditionally independent (or jointly dependent) from a certain within-cluster distribution  $\mathcal{K}(\cdot \mid \theta_k^*)$ , we choose to model  $y_i$  as dependent on another point  $y_j$  that is close by, provided  $y_i$  and  $y_j$  are from the same cluster. This leads to a Markov graphical model based on a spanning forest, a graph consisting of multiple disjoint spanning trees (each tree as a connected subgraph without cycles). The spanning forest itself is not new to statistics. There has been a large literature on using spanning trees and forests for graph estimation, such as Meila and Jordan (2000); Meilă and Jaakkola (2006); Edwards et al. (2010); Byrne and Dawid (2015); Duan and Dunson (2021b); Luo et al. (2021). Nevertheless, a key difference between graph estimation and graph-based clustering is that — the former aims to recover both the node partition and the edges characterizing dependencies, while the latter only focuses on estimating the node partition alone (equivalent to clustering). Therefore, a distinction of our study is that we will treat the edges as a nuisance parameter/latent variable, while we will characterize the node partition in the marginal distribution.

Importantly, we formally show that by marginalizing the randomness of edges, the point estimate on the node partition is provably close to the one from the normalized spectral clustering algorithm. As the result, the spanning forest model can serve as the probabilistic model for the spectral clustering algorithm — this relationship is analogous to the one between the Gaussian mixture model and the K-means algorithm (MacQueen, 1967). Further, we show that treating the spanning forest as random, as opposed to a fixed parameter (that is unknown), leads to much less sensitivity in clustering performance, compared to cutting the minimum spanning tree algorithm (Gower and Ross, 1969).

On the distribution specification on the node and edges, we take a Bayesian non-parametric approach by considering the forest model as realized from a “forest process” —

each cluster is initiated with a point from a root distribution, then gradually grown with new points from a leaf distribution. We characterize the key differences in the partition distribution between the forest and classic Pólya urn processes. This difference also reveals that extra care should be exerted during model specification when using graphical models for clustering.

Lastly, by establishing the probabilistic model counterpart for spectral clustering, we show how such models can be easily extended to incorporate other dependency structures. We demonstrate several extensions, including a multi-subject clustering of the brain networks, and a high-dimensional clustering of photo images.

## 2 Method

### 2.1 Background on Spectral Clustering Algorithms

We first provide a brief review of spectral clustering algorithms. For data  $y_1, \dots, y_n$ , let  $A_{i,j} \geq 0$  be a similarity score between  $y_i$  and  $y_j$ , and denote the degree  $D_{i,i} = \sum_{j \neq i} A_{i,j}$ . To partition the data index  $(1, \dots, n)$  into  $K$  sets,  $\mathcal{V} = (V_1, \dots, V_K)$ , we want to solve the following problem:

$$\min_{\mathcal{V}} \sum_{k=1}^K \frac{\sum_{i \in V_k, j \notin V_k} A_{i,j}}{\sum_{i \in V_k} D_{i,i}}. \quad (1)$$

This is known as the minimum normalized cut loss. The numerator above represents the across-cluster similarity due to cutting  $V_k$  off from the others; and the denominator prevents trivial solutions of forming tiny clusters with small  $\sum_{i \in V_k} D_{i,i}$ .

This optimization problem is a combinatorial problem, hence has motivated approximate solutions such as spectral clustering. To start, using the Laplacian matrix  $L = D - A$  with  $D$  the diagonal matrix of  $D_{i,i}$ 's, and the normalized Laplacian  $N = D^{-1/2} L D^{-1/2}$ , we can equivalently solve the above problem via:

$$\min_{\mathcal{V}} \text{tr}(Z_{\mathcal{V}}' N Z_{\mathcal{V}}),$$

where  $Z_{\mathcal{V}:i,k} = 1(i \in V_k) \sqrt{D_{i,i}} / \sqrt{\sum_{i \in V_k} D_{i,i}}$ . It is not hard to verify that  $Z'_{\mathcal{V}} Z_{\mathcal{V}} = I_K$ . We can obtain a relaxed minimizer of  $Z : Z'Z = I_K$ , by simply taking  $\hat{Z}$  as the bottom  $K$  eigenvectors of  $N$  (with the minimum loss equal to the sum of the smallest  $K$  eigenvalues). Afterward, we cluster the rows of  $\hat{Z}$  into  $K$  groups (using algorithms such as the K-means), hence producing an approximate solution to (1).

To clarify, there is more than one version of the spectral clustering algorithms. An alternative version to (1) is called “minimum ratio cut”, which replaces the denominator  $\sum_{i \in V_k} D_{i,i}$  by the size of cluster  $|V_k|$ . Similarly, continuous relaxation approximation can be obtained by following the same procedures above, except for clustering the eigenvectors of the unnormalized  $L$ . Details on comparing those two versions can be found in Von Luxburg (2007). In this article, we focus on the one based on (1) and the normalized Laplacian matrix  $N$ . This version is also commonly referred to as “normalized spectral clustering”.

## 2.2 Probabilistic Model via Bayesian Spanning Forest

The next question is if there is some partition-based generative model for  $y$ , that has the maximum likelihood estimate (or, the posterior mode in the Bayesian framework) almost the same as the point estimate from the normalized spectral clustering.

We found an almost equivalence in the spanning forest model. A spanning forest model is a special Bayesian network that describes the conditional dependencies among  $y_1, \dots, y_n$ . Given a partition  $\mathcal{V} = (V_1, \dots, V_K)$  of the data index  $(1, \dots, n)$ , consider a forest graph  $\mathcal{F}_{\mathcal{V}} = (T_1, \dots, T_k)$ , with each  $T_k = (V_k, E_k)$  a component tree (a connected subgraph without cycles),  $V_k$  the set of nodes and  $E_k$  the set of edges among  $V_k$ . Using  $\mathcal{F}_{\mathcal{V}}$  and a set of root nodes  $\mathcal{R}_{\mathcal{V}} = (1^*, \dots, K^*)$  with  $k^* \in V_k$ , we can form a graphical model with a conditional likelihood given the forest:

$$\mathcal{L}(y; \mathcal{V}, \mathcal{F}_{\mathcal{V}}, \mathcal{R}_{\mathcal{V}}, \theta) = \prod_{k=1}^K \left[ r(y_{k^*}; \theta) \prod_{(i,j) \in T_k} f(y_i | y_j; \theta) \right], \quad (2)$$

where we refer to  $r(\cdot; \theta)$  as a “root” distribution, and  $f(\cdot | y_j; \theta)$  as a “leaf” distribution; and we use  $\theta$  to denote the other parameter; and we use simplified notation  $(i, j) \in G$  to mean that  $(i, j)$  is an edge of the graph  $G$ .

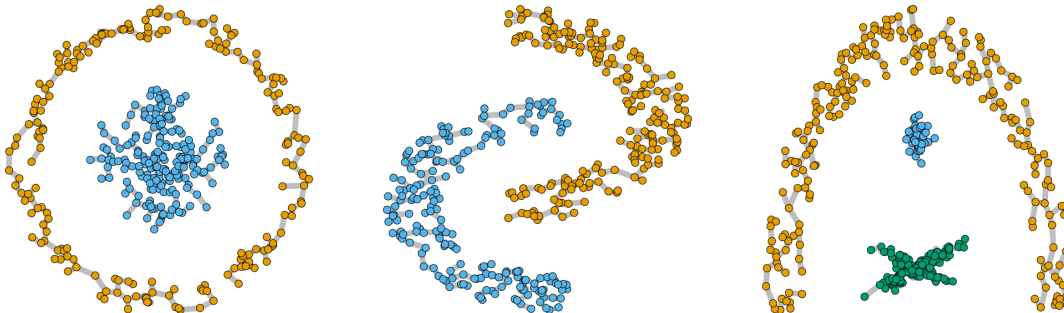


Figure 1: Three examples of clusters that can be represented by a spanning forest. Figure 1 illustrates the high flexibility of a spanning forest in representing clusters. It shows the sampled  $\mathcal{F}$  based on three clustering benchmark datasets. Note that some clusters are not elliptical or convex in shape. Rather, each cluster can be imagined as if it were formed by connecting a point to another nearby.

**Remark 1** *To clarify, the point estimation on a spanning forest (as some fixed and unknown graph) has been studied (Gower and Ross, 1969). However, a distinction here is that we consider  $\mathcal{V}$  as the parameter of interest, but the edges and roots  $(\mathcal{F}_{\mathcal{V}}, \mathcal{R}_{\mathcal{V}})$  as latent variables. The performance differences are shown in the Supplementary Materials S4.6.*

The stochastic view of  $(\mathcal{F}_{\mathcal{V}}, \mathcal{R}_{\mathcal{V}})$  is important, as it allows us to incorporate the uncertainty of edges and avoids the sensitivity issue in the point graph estimate. Equivalently, our clustering model is based on the marginal likelihood that varies with the node partition  $\mathcal{V}$ :

$$\mathcal{L}(y; \mathcal{V}, \theta) = \sum_{\mathcal{F}_{\mathcal{V}}, \mathcal{R}_{\mathcal{V}}} \mathcal{L}(y; \mathcal{V}, \mathcal{F}_{\mathcal{V}}, \mathcal{R}_{\mathcal{V}}, \theta) \Pi(\mathcal{F}_{\mathcal{V}}, \mathcal{R}_{\mathcal{V}} | \mathcal{V}). \quad (3)$$

where  $\Pi(\mathcal{F}_{\mathcal{V}}, \mathcal{R}_{\mathcal{V}} | \mathcal{V})$  is the latent variable distribution that we will specify in the next section. We can quantify the marginal connecting probability for each potential edge  $(i, j)$ :

$$M_{i,j} := \Pr[F_{\mathcal{V}} \ni (i, j)] \propto \sum_{\mathcal{V}} \sum_{\mathcal{F}_{\mathcal{V}}, \mathcal{R}_{\mathcal{V}}} 1[(i, j) \in F_{\mathcal{V}}] \mathcal{L}(y; \mathcal{V}, \mathcal{F}_{\mathcal{V}}, \mathcal{R}_{\mathcal{V}}, \theta) \Pi(\mathcal{F}_{\mathcal{V}}, \mathcal{R}_{\mathcal{V}} | \mathcal{V}). \quad (4)$$



Similar to the normalized graph cut, there is no closed-form solution for directly maximizing (3). However, closed-form does exist for (4) (see Section 4). Therefore, an approximate maximizer of (3),  $\hat{\mathcal{V}}$ , can be obtained via computing the matrix  $M$  and searching for  $K$  diagonal blocks (after row and column index permutation) that contain the highest total values of  $M_{i,j}$ 's. Specifically, we can extract the top leading eigenvectors of  $M$  and cluster the rows into  $K$  groups.

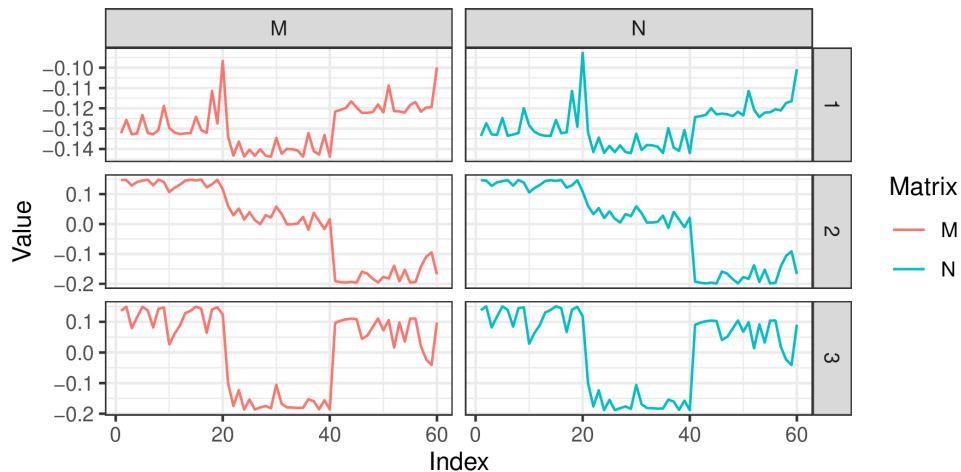


Figure 2: Comparing the eigenvectors of a marginal connecting probability matrix  $M$  and the ones of normalized Laplacian  $N$ .

This approximate marginal likelihood maximizer produces almost the same estimate as the normalized spectral clustering does. This is because the two sets of eigenvectors are almost the same. Further, it is important to clarify that such closeness does not depend on how the data are really generated. Therefore, to provide some numerical evidence, for simplicity, we generate  $y_i$  from a simple three-component Gaussian mixture in  $\mathbb{R}^2$  with means in  $(0, 0)$ ,  $(2, 2)$ ,  $(4, 4)$  and all variances equal to  $I_2$ . Figure 2 compares the eigenvectors of the matrix  $M$  and the normalized Laplacian  $N$  (that uses  $f$  and  $r$  to specify  $A$ , with details provided in Section 4). Clearly, these two are almost identical in values. Due to this connection, the clustering estimates from spectral clustering can be viewed as an

approximate estimate for  $\hat{\mathcal{V}}$  in (3).

We now fully specify the Bayesian forest model. For simplicity, we now focus on continuous  $y_i \in \mathbb{R}^p$ . For ease of computation, we recommend choosing  $f$  as a symmetric function  $f(y_i | y_j; \theta) = f(y_j | y_i; \theta)$ , so that the likelihood is invariant to the direction of each edge; and choose  $r$  as a diffuse density, so that the likelihood is less sensitive to the choice of a node as root. In this article, we choose a Gaussian density for  $f$  and Cauchy for  $r$ :

$$\begin{aligned} f(y_i | y_j; \theta) &= (2\pi\sigma_{i,j})^{-p/2} \exp \left\{ -\frac{\|y_i - y_j\|_2^2}{2\sigma_{i,j}} \right\}, \\ r(y_i; \theta) &= \frac{\Gamma[(1+p)/2]}{\gamma^p \pi^{(1+p)/2}} \frac{1}{(1 + \|y_i - \mu\|_2^2 / \gamma^2)^{(1+p)/2}}. \end{aligned} \tag{5}$$

where  $\sigma_{ij} > 0$  and  $\gamma > 0$  are scale parameters. As the magnitudes of distances between neighboring points may differ significantly from cluster to cluster, we use a local parameterization  $\sigma_{i,j} = \tilde{\sigma}_i \tilde{\sigma}_j$ , and will regularize  $(\tilde{\sigma}_1, \dots, \tilde{\sigma}_n)$  via a hyper-prior.

**Remark 2** *In (5), we effectively use Euclidean distances  $\|y_i - y_j\|_2$ . We focus on Euclidean distance in the main text, for the simplicity of presentation and to allow a complete specification of priors. One can replace Euclidean distance with some others, such as Mahalanobis distance and geodesic distance. We present a case of high-dimensional clustering based on geodesic distance on the unit-sphere in the Supplementary Materials S1.1.*

### 2.3 Forest Process and Product Partition Prior

To simplify notations as well as to facilitate computation, we now introduce an auxiliary node 0 that connects to all roots  $(1^*, \dots, K^*)$ . As the result, the model can be equivalently represented by a spanning tree rooted at 0:

$$\mathcal{T} = (V_{\mathcal{T}}, E_{\mathcal{T}}),$$

$$V_{\mathcal{T}} = \{0\} \cup V_1 \cup \dots \cup V_K, \quad E_{\mathcal{T}} = \{(0, 1^*), \dots, (0, K^*)\} \cup E_1 \cup \dots \cup E_K.$$

In this section, we focus on the distribution specification for  $\mathcal{T}$ . The distribution, denoted by  $\Pi(\mathcal{T})$ ,  $\Pi(\mathcal{T})$  can be factorized according to the following hierarchies: picking the number

of partitions  $K$ , partitioning the nodes into  $(V_1, \dots, V_K)$ , forming edges  $E_k$  and picking one root  $k^*$  for each  $V_k$ . To be clear on the nomenclature, we call  $\Pi(\mathcal{F}_{\mathcal{V}}, \mathcal{R}_{\mathcal{V}} | \mathcal{V})$  as the “latent variable distribution”,  $\Pi_0(\mathcal{V})$  as the “partition prior”.

$$\Pi(\mathcal{T}) = \underbrace{\left\{ \Pi_0(K) \Pi_0(V_1, \dots, V_K | K) \right\}}_{\Pi_0(\mathcal{V})} \prod_{k=1}^K \underbrace{\left\{ \Pi(E_k | V_k) \Pi(k^* | E_k, V_k) \right\}}_{\Pi(\mathcal{F}_{\mathcal{V}}, \mathcal{R}_{\mathcal{V}} | \mathcal{V})}. \quad (6)$$

**Remark 3** *In Bayesian non-parametric literature,  $\Pi_0(K) \Pi_0(V_1, \dots, V_K | K)$  is known as the partition probability function, which plays the key role in controlling cluster sizes and cluster number in model-based clustering. However, when it comes to graphical model-based clustering (such as our forest model), it is important to note the difference — for each partition  $V_k$ , there is an additional probability  $\Pi(E_k, k^* | V_k)$  due to the multiplicity of all possible subgraphs formed between the nodes in  $V_k$ .*

For simplicity, we will use discrete uniform distribution for  $\Pi(E_k, k^* | V_k)$ . Since there are  $n_k^{(n_k-2)_+}$  possible spanning trees for  $n_k$  nodes [ $(x)_+ = x$  if  $x > 0$ , otherwise 0], and  $n_k$  possible choice of roots. We have  $\Pi(E_k, k^* | V_k) = n_k^{-(n_k-1)}$ .

We now discuss two different ways to complete the distribution specification. We first take a “ground-up” approach by viewing  $\mathcal{T}$  as from a stochastic process where the node number  $n$  could grow indefinitely. Starting from the first edge  $e_1 = (0, 1)$ , we sequentially draw new edges and add to  $\mathcal{T}$ , from

$$e_i | e_1, \dots, e_{i-1} \sim \sum_{j=1}^{i-1} \pi_j^{[i]} \delta_{(j,i)}(\cdot) + \pi_i^{[i]} \delta_{(0,i)}(\cdot), \quad (7)$$

$$y_i | (j, i) \sim 1(j \geq 1) f(\cdot | y_j) + 1(j = 0) r(\cdot),$$

with some probability vector  $(\pi_1^{[i]}, \dots, \pi_i^{[i]})$  that adds up to one. We refer to (7) as a forest process. The forest process is a generalization of the Pólya urn process (Blackwell and MacQueen, 1973). For the latter,  $e_i = (j, i)$  would make node  $i$  take the same value as

node  $j$ ,  $y_i = y_j$  [although in model-based clustering, one would use notation  $\theta_i = \theta_j$ , and  $y_i \sim \mathcal{K}(\cdot | \theta_i)$ ];  $e_i = (0, i)$  would make node  $i$  draw a new value for  $y_i$  from the base distribution. Due to this relationship, we can borrow popular parameterization for  $\pi_j^{[i]}$  from the urn process literature. For example, we can use the Chinese restaurant process parameterization  $\pi_j^{[i]} = 1/(i - 1 + \alpha)$  for  $j = 1, \dots, (i - 1)$ , and  $\pi_i^{[i]} = \alpha/(i - 1 + \alpha)$  with some chosen  $\alpha > 0$ . After marginalizing over the order of  $i$  and partition index [see Miller (2019) for a simplified proof of the partition function], we obtain:

$$\Pi(\mathcal{T}) = \frac{\alpha^K \Gamma(\alpha)}{\Gamma(\alpha + n)} \prod_{k=1}^K \Gamma(n_k) n_k^{-(n_k-1)}. \quad (8)$$

Compared to the partition probability prior in the Chinese restaurant process, we have an additional  $n_k^{-(n_k-1)}$  term that corresponds to the conditional prior weight of for each possible  $(k^*, E_k)$  given a partition  $V_k$ .

To help understand the effect of this additional term on the posterior, we can imagine two extreme possibilities in the conditional likelihood given a  $V_k$ . If the conditional  $\mathcal{L}(y_i : i \in V_k | k^*, E_k)$  is skewed toward one particular choice of tree  $(\hat{k}^*, \hat{E}_k)$  [that is,  $\mathcal{L}(y_i : i \in V_k | k^*, E_k)$  is large when  $(k^*, E_k) = (\hat{k}^*, \hat{E}_k)$ , but is close to zero for other values of  $(k^*, E_k)$ ], then  $n_k^{-(n_k-1)}$  acts as a penalty for a lack of diversity in trees. On the other hand, if  $\mathcal{L}(y_i : i \in V_k | k^*, E_k)$  is equal for all possible  $(k^*, E_k)$ 's, then we can simply marginalize over  $(k^*, E_k)$  and be not be subject to this penalty [since  $\sum_{(k^*, E_k)} n_k^{-(n_k-1)} = 1$ ].

Therefore, we can form an intuition by interpolating those two extremes: if a set of data points (of size  $n_k$ ) are “well-knit” such that they can be connected via many possible spanning trees (each with a high conditional likelihood), then it would have a higher posterior probability of being clustered together, compared to some other points (of the same size  $n_k$ ) that have only a few trees with high conditional likelihood.

With the “ground-up” construction useful for understanding the difference from the

classic urn process, the distribution (8) itself is not very convenient for posterior computation. Therefore, we also explore the alternative of a “top-down” approach. This is based on directly assigning a product partition probability (Hartigan, 1990; Barry and Hartigan, 1993; Crowley, 1997; Quintana and Iglesias, 2003) as

$$\Pi_0(V_1, \dots, V_K | K) = \frac{\prod_{k=1}^K n_k^{(n_k-1)}}{\sum_{\text{all } (V_1^*, \dots, V_K^*)} \prod_{k=1}^K |V_k^*|^{(|V_k^*|-1)}}, \quad (9)$$

where the cohesion function  $n_k^{(n_k-1)}$  effectively cancels out the probability for each  $(k^*, E_k)$ .

To assign a prior for  $K$ , we assign a probability

$$\Pi_0(K) \propto \lambda^K \sum_{\text{all } (V_1^*, \dots, V_K^*)} \prod_{k=1}^K |V_k^*|^{(|V_k^*|-1)},$$

supported on  $K \in \{1, \dots, n\}$  with  $\lambda > 0$ , with  $\Pi(E_k, k^* | V_k) = n_k^{-(n_k-1)}$ , multiplying the terms according to (6) leads to

$$\Pi(\mathcal{T}) \propto \lambda^K, \quad (10)$$

which is similar to a truncated geometric distribution and easy to handle in posterior computation, and we will use this from now on. In this article, we set  $\lambda = 0.5$ .

**Remark 4** *We now discuss the exchangeability of the sequence of random variables generated from the above forest process. The exchangeability is defined as the invariance of distribution  $\Pi(X_1 = x_1, \dots, X_n = x_n) = \Pi(X_1 = x_{\tilde{\pi}_1}, \dots, X_n = x_{\tilde{\pi}_n})$  under any permutation  $(\tilde{\pi}_1, \dots, \tilde{\pi}_n)$  (Diaconis, 1977). For simplicity, we focus on the joint distribution with  $\theta$  marginalized out. There are three categories of random variables associated with each node index  $i$ : the first drawn edge  $(j, i)$  that points to a new node  $i$  (whose sequence forms  $\mathcal{T} = (\mathcal{V}, \{E_k, k^*\}_{k=1}^K)$ ), the cluster assignment of a node  $c_i$  (whose sequence forms  $\mathcal{V}$ ), and the data point  $y_i$ . It is not hard to see that, since each component tree encodes an order among  $\{i : c_i = k\}$ , the joint distribution of the data and the forest  $\Pi(y_1, \dots, y_n, \mathcal{T})$  is*

not exchangeable. Nevertheless, as we marginalize out each  $(E_k, k^*)$  to form the clustering likelihood  $\mathcal{L}(y; \mathcal{V})$  as in (3), and all priors  $\Pi_0(\mathcal{V})$  presented in this section only depend on the number and sizes of clusters, the joint distribution of the data and cluster labels  $\Pi\{(y_1, c_1), \dots, (y_n, c_n)\} = \mathcal{L}(y_i; \mathcal{V})\Pi_0(\mathcal{V})$  is exchangeable. Further, we could marginalize over  $\mathcal{V}$ , and see that  $\Pi(y_1, \dots, y_n)$  is exchangeable.

## 2.4 Hyper-priors for the Other Parameters

We now specify the hyper-priors for the parameters in the root and leaf densities. To avoid model sensitivities to scaling and shifting of the data, we assume that the data have been appropriately scaled and centered (for example, via standardization), so that the marginally  $\mathbb{E}y \approx 0$  and  $\mathbb{E}\|y_{\cdot,j} - \mathbb{E}y_{\cdot,j}\|_2^2 \approx 1$  for  $j = 1, \dots, p$ . To make the root density  $r(\cdot)$  close to a small constant in the support of the data, we set  $\mu = 0$  and  $\gamma^2 \sim \text{Inverse-Gamma}(2, 1)$ .

For  $\sigma_{i,j}$  in the leaf density  $f(y_i | y_j; \sigma_{i,j})$ , in order to likely pick an edge  $(i, j)$  with  $j$  as a close neighbors of  $i$  (that is,  $(i, j)$  with small  $\|y_i - y_j\|_2$ ), we want most of  $\sigma_{i,j} = \tilde{\sigma}_i \tilde{\sigma}_j$  to be small. We use the following hierarchical inverse-gamma prior that shrinks each  $\tilde{\sigma}_i$ , while using a common scale hyper-parameter  $\beta_\sigma$  to borrow strengths among  $\tilde{\sigma}_i$ 's,

$$\begin{aligned} \beta_\sigma &\sim \text{Exp}(\eta_\sigma), & \eta_\sigma &\sim \text{Inverse-Gamma}(a_\sigma, \xi_\sigma), \\ \tilde{\sigma}_i &\stackrel{iid}{\sim} \text{Inverse-Gamma}(b_\sigma, \beta_\sigma) \text{ for } i = 1, \dots, n, \end{aligned}$$

where  $\eta_\sigma$  is the scale parameter for the exponential. To induce a shrinkage effect *a priori*, we use  $a_\sigma = 100$  and  $\xi_\sigma = 1$  for a likely small  $\eta_\sigma$  hence a small  $\beta_\sigma$ . Further, we note that the coefficient of variation  $\sqrt{\text{Var}(\tilde{\sigma}_i | \beta_\sigma)}/\mathbb{E}(\tilde{\sigma}_i | \beta_\sigma) = 1/\sqrt{b_\sigma - 2}$ ; therefore, we set  $b_\sigma = 10$  to have most of  $\tilde{\sigma}_i$  near  $\mathbb{E}(\tilde{\sigma}_i | \beta_\sigma) = \beta_\sigma/(b_\sigma - 1)$  in the prior. We use these hyper-prior settings in all the examples presented in this article.

In addition, Zelnik-Manor and Perona (2005) show good empirical performance in spectral clustering, based on a heuristic of setting  $\tilde{\sigma}_i$  to a low order statistic of the distances to

$y_i$ . We develop a model-based formalization that achieves similar effects. Since the model is more involved than a simple Bayesian spanning forest model, we defer the details to the Supplementary Materials S5.

## 2.5 Model-based Extensions

Compared to algorithms, a major advantage of probabilistic models is the ease of building useful model-based extensions. We demonstrate three directions for extending the Bayesian forest model. Due to the page constraint, we defer the details and numeric results of the first two extensions in the Supplementary Materials S1.1 and S1.2.

**Latent Forest Model:** First, one could use the realization of the forest process as latent variables in another model  $\mathcal{M}$  for data  $(y_1, \dots, y_n)$ ,

$$z_1, \dots, z_n \sim \text{Forest Model}(\mathcal{T}; \theta_z), \quad y_1, \dots, y_n \sim \mathcal{M}(z_1, \dots, z_n; \theta_y),$$

where  $\theta_z$  and  $\theta_y$  denote the other needed parameters. For example, for clustering high-dimensional data such as images, it is often necessary to represent each high-dimensional observation  $y_i$  by a low-dimensional coordinate  $z_i$  (Wu et al., 2014; Chandra et al., 2020).

In the Supplementary Materials, we present a high-dimensional clustering model, using an autoregressive matrix Gaussian for  $\mathcal{M}$  and a sparse von Mises-Fisher for the forest model.

**Informative Prior–Latent Variable Distribution:** Second, in applications it is sometimes desirable to have the clustering dependent on some external information  $x$ , such as covariates (Müller et al., 2011) or an existing partition (Paganin et al., 2021). From a Bayesian view, this can be achieved via taking an  $x$ -informative distribution:

$$\mathcal{T} \sim \Pi(\cdot | x), \quad y_1, \dots, y_n \sim \text{Forest Model}(\mathcal{T}; \theta).$$

In the Supplementary Materials, we illustrate an extension with a covariate-dependent product partition model [PPM $x$ , Müller et al. (2011)] into the distribution of  $\mathcal{T}$ .

**Hierarchical Multi-view Clustering:** Third, for multi-subject data  $(y_1^{(s)}, \dots, y_n^{(s)})$  for  $s = 1, \dots, S$ , we want to find a clustering for every  $s$ . At the same time, we can borrow strength among subjects, by letting subjects share some similar partition structure on a subset of nodes (while differing on the other nodes). This is known as multi-view clustering. On the other hand, a challenge is that a forest is a discrete object subject to combinatorial constraints, hence it would be difficult to partition the nodes freely while accommodating the tree structure. To circumvent this issue, we propose a latent coordinate-based distribution that gives a continuous representation for  $\mathcal{T}^{(s)}$ . Consider a latent  $z_i^{(s)} \in \mathbb{R}^d$  for each node  $i = 1, \dots, n$ , we assign a joint prior–latent variable distribution for  $z^{(s)}$  and  $\mathcal{T}^{(s)}$ :

$$\begin{aligned} \Pi[z^{(s)}, \mathcal{T}^{(s)}] &\propto \\ \lambda^{K[\mathcal{T}^{(s)}]} &\left[ \prod_{(i,j) \in \mathcal{T}^{(s)}: i \geq 1, j \geq 1} \exp\left(-\frac{\|z_i^{(s)} - z_j^{(s)}\|_2^2}{2\rho}\right) \right] \left[ \prod_{i=1}^n \left\{ \sum_{k=1}^{\tilde{\kappa}} v_{i,k} \exp\left(-\frac{\|z_i^{(s)} - \eta_k^*\|_2^2}{2\sigma_z^2}\right) \right\} \right], \quad (11) \\ (v_{i,1}, \dots, v_{i,\tilde{\kappa}}) &\sim \text{Dir}(1/\tilde{\kappa}, \dots, 1/\tilde{\kappa}) \quad \text{for } i = 1, \dots, n, \\ \{y_1^{(s)}, \dots, y_n^{(s)}\} &\sim \text{Forest Model}(\mathcal{T}^{(s)}) \quad \text{for } s = 1, \dots, S, \end{aligned}$$

where  $v_{i,1}, \dots, v_{i,\tilde{\kappa}}$  are the weights that vary with  $i$  and  $\sum_{k=1}^{\tilde{\kappa}} v_{i,k} = 1$ ,  $\rho > 0$ , and  $z^{(s)} \in \mathbb{R}^{n \times d}$  is the matrix form. Equivalently, the above assigns each node a location parameter  $\eta_i^{(s)}$ , drawn from a hierarchical Dirichlet distribution with shared atoms  $\{\eta_1^*, \dots, \eta_{\tilde{\kappa}}^*\}$  and probability  $(v_{\cdot,1}, \dots, v_{\cdot,\tilde{\kappa}})$  (Teh et al., 2006). Further, one could let  $\eta_k^*$  vary over node according to some functional using a hybrid Dirichlet distribution (Petroni et al., 2009).

Using a Gaussian mixture kernel on  $z_i^{(s)}$ , we can now separate  $z_i^{(s)}$ 's into several groups that are far apart. To make the parameters identifiable and have large separations between groups, we fix  $\tilde{\eta}_k^*$ 's on the  $d$ -dimensional integer lattice  $\{0, 1, 2\}^d$  with  $d = 2$  (hence  $\tilde{\kappa} = 9$ ); and we use  $\sigma_z^2 = 0.01$  and  $\rho = 0.001$  in this article.

**Remark 5** *To clarify, our goal is to induce between-subject similarity in the node partition,*



not the tree structure. For example, for two subjects  $s$  and  $s'$ , when  $z_i^{(s)}$  and  $z_i^{(s')}$  are both near  $\eta_k^*$  for all  $i \in C$ , then both the spanning forest  $\mathcal{T}^{(s)}$  and  $\mathcal{T}^{(s')}$  will likely cluster the nodes in  $C$  together, even though  $T_k^{(s)}$  and  $T_k^{(s')}$  associated with  $V_k \supset C$  may be different.

The posterior can be sampled efficiently using the Gibbs sampling algorithm. We provide the posterior sampling algorithm in the Supplementary Materials S1.3, and illustrate this model in Section 6 of modeling brain regions for multiple subjects.

## 3 Posterior Computation

### 3.1 Gibbs Sampling Algorithm

We now describe the Markov chain Monte Carlo (MCMC) algorithm. For ease of notation, we use an  $(n+1) \times (n+1)$  matrix  $S$ , with  $S_{i,j} = \log f(y_i | y_j; \theta)$ ,  $S_{0,i} = S_{i,0} = \log r(y_i; \theta) + \log \lambda$  (for convenience, we use 0 to index the last row/column),  $S_{i,i} = 0$ , and  $A_{\mathcal{T}}$  to represent the adjacency matrix of  $\mathcal{T}$ . We have the posterior distribution

$$\Pi(\mathcal{T}, \theta | y) \propto \exp \{ \text{tr}[S(\theta)A_{\mathcal{T}}]/2 \} \Pi_0(\theta). \quad (12)$$

Note the above form conveniently include the prior term for the number of clusters,  $\lambda^K$ , via the number of edges adjacent to node 0.

Our MCMC algorithm alternates in updating  $\mathcal{T}$  and  $\theta$ , hence is a Gibbs sampling algorithm. To sample  $\mathcal{T}$  given  $\theta$ , we take the random-walk covering algorithm for weighted spanning tree (Mosbah and Saheb, 1999), as an extension of the Andrei–Broder algorithm for sampling uniform spanning tree (Broder, 1989; Aldous, 1990). For this article to be self-contained, we describe the algorithm below. The above algorithm produces a random sample  $\mathcal{T}$  following the full conditional  $\Pi(\mathcal{T} | \theta, y)$  proportional to (12). It has an expected finish time of  $O(n \log n)$ . Although some faster algorithms have been developed (Schild, 2018), we choose to present the random-walk covering algorithm for its simplicity.

---

**Algorithm 1** Random-walk covering algorithm for sampling the augmented tree  $\mathcal{T}$ .

---

Start with  $V_{\mathcal{T}} = \{0\}$  and  $E_{\mathcal{T}} = \emptyset$ , and set  $i \leftarrow 0$ :

**while**  $|V_{\mathcal{T}}| \neq n + 1$  **do**

Take a random walk from  $i$  to  $j$  with probability  $\Pr(j \mid i) = \frac{\exp[S_{i,j}(\theta)]}{\sum_{j:j \neq i} \exp[S_{i,j}(\theta)]}$ .

**if**  $j \notin V_{\mathcal{T}}$  **then**

Add  $j$  to  $V_{\mathcal{T}}$ . Add  $(i, j)$  to  $E_{\mathcal{T}}$ .

Update  $i \leftarrow j$ .

---

We sample  $\tilde{\sigma}_i$  using the following steps,

$$\begin{aligned} (\eta_{\sigma} \mid \cdot) &\sim \text{Inverse-Gamma}(1 + a_{\sigma}, \beta_{\sigma} + \xi_{\sigma}) \\ (\beta_{\sigma} \mid \cdot) &\sim \text{Gamma}\left\{1 + nb_{\sigma}, \left(\sum_{i=1}^n \frac{1}{\tilde{\sigma}_i} + \frac{1}{\eta_{\sigma}}\right)^{-1}\right\} \\ (\tilde{\sigma}_i \mid \cdot) &\sim \text{Inverse-Gamma}\left[\frac{p \sum_j 1\{(i, j) \in \mathcal{T}\}}{2} + b_{\sigma}, \sum_{j:(i,j) \in \mathcal{T}} \frac{\|y_i - y_j\|_2^2}{2\tilde{\sigma}_j} + \beta_{\sigma}\right] \end{aligned}$$

To update  $\gamma$ , we use the form of the multivariate Cauchy as a scale mixture of  $N(\mu, \gamma^2 u_{\gamma,i} I_p)$

over  $u_{\gamma,i} \sim \text{Inverse-Gamma}(1/2, 1/2)$ . We can update via

$$\begin{aligned} u_{\gamma,i} &\sim \text{Inverse-Gamma}\left(\frac{1+p}{2}, \frac{1}{2} + \frac{\|y_i - \mu\|_2^2}{2\gamma^2}\right), \\ \gamma^2 &\sim \text{Inverse-Gamma}\left(2 + \frac{Kp}{2}, \hat{\sigma}_y^2 + \sum_{i:(0,i) \in \mathcal{T}} \frac{\|y_i - \mu\|_2^2}{2u_{\gamma,i}}\right). \end{aligned}$$

We run the MCMC algorithm iteratively for many iterations. And we discard the first half of iterations as burn-in.

**Remark 6** *We want to emphasize that the Andrei–Broder random-walk covering algorithm (Broder, 1989; Aldous, 1990; Mosbah and Saheb, 1999) is an exact algorithm for sampling a spanning tree  $\mathcal{T}$ . That is, if  $\theta$  were fixed, each run of this algorithm would produce an independent Monte Carlo sample  $\mathcal{T} \sim \Pi(\mathcal{T} \mid \theta, y)$ . Removing the auxiliary node 0 from  $\mathcal{T}$  will produce  $K$  disjoint spanning trees. This augmented graph technique is inspired by Boykov et al. (2001).*

*In our algorithm, since the scale parameters in  $\theta$  are unknown, we use Markov chain Monte Carlo that updates two sets of parameters, (i)  $(\theta_{[t+1]} \mid \mathcal{T}_{[t]})$  and (ii)  $(\mathcal{T}_{[t+1]} \mid \theta_{[t+1]})$  from iteration  $[t]$  to  $[t + 1]$ . Therefore, rigorously speaking, there is a Markov chain dependency between  $\mathcal{T}_{[t]}$  and  $\mathcal{T}_{[t+1]}$  induced by  $\theta_{[t+1]}$ . Nevertheless, since we draw  $\mathcal{T}$  in a block via the random-walk covering algorithm, we empirically find that  $\mathcal{T}_{[t+1]}$  and  $\mathcal{T}_{[t]}$  are substantially different. In the Supplementary Materials S4.4, we quantify the iteration-to-iteration graph changes, and provide diagnostics with multiple start points of  $(\mathcal{T}_{[0]}, \theta_{[0]})$ .*

### 3.2 Posterior Point Estimate on Clustering

In the field of Bayesian clustering, for producing point estimate on the partition, it had been a long-time practice to simply track  $\text{pr}(c_i = k \mid y)$ , then take the element-wise posterior mode over  $k$  as the point estimate for  $\hat{c}_i$ . Nevertheless, this was shown to be sub-optimal due to that: (i) label switching issue causes unreliable estimates on  $\text{pr}(c_i = k \mid y)$ ; (ii) the element-wise mode can be unrepresentative of the center of distribution for  $(c_1, \dots, c_n)$  (Wade and Ghahramani, 2018). These weaknesses have motivated new methods of obtaining point estimate of clustering, that transform an  $n \times n$  pairwise co-assignment matrix  $\{\text{pr}(c_i = c_j \mid y)\}_{\text{all } (i,j)}$  into an  $n \times K$  assignment matrix (Medvedovic and Sivaganesan, 2002; Rasmussen et al., 2008; Molitor et al., 2010; Wade and Ghahramani, 2018). More broadly speaking, minimizing a loss function based on the posterior sample (via some estimator or algorithm) is common for producing a point estimate under some decision theory criterion. For example, the posterior mean comes as the minimizer of the squared error loss; in Bayesian factor modeling, an orthogonal Procrustes-based loss function is used for producing the posterior summary of the loading matrix from the generated MCMC samples (Abmann et al., 2016).

We follow this strategy. There have been many algorithms that one could use. For a recent survey, see Dahl et al. (2022). In this article, we use a simple solution of first

finding the mode of  $K$  from the posterior sample, then doing a  $\hat{K}$ -rank symmetric matrix factorization on  $\{\text{pr}(c_i = c_j \mid y)\}_{\text{all } (i,j)}$  and clustering into  $\hat{K}$  groups, provided by RcppML package (DeBruine et al., 2021).

## 4 Theoretical Properties

### 4.1 Convergence of Eigenvectors

We now formalize the closeness of the eigenvectors of matrices  $N$  and  $M$  (shown in Section 2.2), by establishing the convergence of the two sets of eigenvectors as  $n$  increases.

To be specific, we focus on the normalized spectral clustering algorithm using the similarity  $A_{i,j} = \exp(S_{i,j})$ , with  $S_{i,j} = \log f(y_i \mid y_j; \theta)$ ,  $S_{0,i} = S_{i,0} = \log r(y_i; \theta) + \log \lambda$ . On the other hand, for the specific form,  $f(y_i \mid y_j)$  can be any density satisfying  $f(y_i \mid y_j, \theta) = f(y_j \mid y_i, \theta)$ ,  $r(y_i; \theta)$  can be any density satisfying  $r(y_i; \theta) > 0$ . For the associated normalized Laplacian  $N$ , we denote the first  $K$  bottom eigenvectors by  $\phi_1, \dots, \phi_K$ , which correspond to the smallest  $K$  eigenvalues.

Let  $M$  be the matrix with  $M_{i,j} = \text{pr}[\mathcal{T} \ni (i, j) \mid y, \theta]$  for  $i \neq j$  and  $M_{i,i} = 0$ . The Kirchhoff's tree theorem (Chaiken and Kleitman, 1978) gives an enumeration of all  $\mathcal{T} \in \mathbb{T}$ ,

$$\sum_{\mathcal{T} \in \mathbb{T}} \prod_{(i,j) \in \mathcal{T}} \exp(S_{i,j}) = (n+1)^{-1} \prod_{h=2}^{n+1} \lambda_{(h)}(L) \quad (13)$$

where  $L$  is the Laplacian matrix transform of the similarity matrix  $A$ ;  $\lambda_{(h)}$  denotes the  $h$ th smallest eigenvalue. Differentiating its logarithmic transform with respect to  $S_{i,j}$ ,

$$M_{i,j} = \text{Pr}[\mathcal{T} \ni (i, j) \mid y] = \frac{\sum_{\mathcal{T} \in \mathbb{T}, (i,j) \in \mathcal{T}} \prod_{(i',j') \in \mathcal{T}} \exp(S_{i',j'})}{\sum_{\mathcal{T} \in \mathbb{T}} \prod_{(i',j') \in \mathcal{T}} \exp(S_{i',j'})} = \frac{\partial \sum_{i=2}^{n+1} \log \lambda_{(i)}(L)}{\partial S_{i,j}}.$$

Let  $\Psi_1, \dots, \Psi_K$  be the top  $K$  eigenvectors of  $M$ , associated with eigenvalues  $\xi_1 \geq \xi_2 \geq \dots \geq \xi_K$ , and  $\xi_K > \xi_{K+1} \geq \xi_{K+2} \geq \dots \geq \xi_{n+1}$ . And we can compare with the  $K$  leading eigenvectors of  $(-N) \in \mathbb{R}^{n \times n}$ ,  $\phi_1, \dots, \phi_K$ . Using  $\Psi_{1:K}$  and  $\phi_{1:K}$  to denote two  $(n+1) \times K$  matrices, we now show they are close to each other.

**Theorem 1** *There exists an orthonormal matrix  $R \in \mathbb{R}^{K \times K}$  and a finite constant  $\epsilon > 0$ ,*

$$\|\Psi_{1:K} - \phi_{1:K} R\|_F \leq \frac{40\sqrt{K(n+1)}}{\xi_K - \xi_{K+1}} \max_{i,j} \left\{ (1 + \epsilon)(D_i^{-1/2} - D_j^{-1/2})^2 A_{i,j} \right\},$$

*with probability at least  $1 - \exp(-n)$ .*

**Remark 7** *To make the right-hand side go to zero, a sufficient condition is to have all  $A_{i,j}/D_{i,i} = O(n^{-\kappa})$  with  $\kappa > 1/2$ . We provide a detailed definition of the bound constant  $\epsilon$  in the Supplementary Materials S2.*

*To explain the intuition behind this theorem, our starting point is the close relationship between Laplacian and spanning tree models — multiplying both sides of Equation (13) by  $(n+1)^{-(n-1)}$  shows that the non-zero eigenvalue product of the graph Laplacian  $L$  is proportional to the marginal probability of  $n$  data points from a spanning forest-mixture model. Starting from this equality, we can write the marginal inclusion probability matrix of  $\mathcal{T}$  as a mildly perturbed form of the normalized Laplacian matrix. Intuitively, when two matrices are close, their eigenvectors will be close as well (Yu et al., 2015).*

Therefore, under mild conditions, as  $n \rightarrow \infty$ , the two sets of leading eigenvectors converge. In the Supplementary Materials S4.7, we show that the convergence is very fast, with the two sets of leading eigenvectors becoming almost indistinguishable starting around  $n \geq 50$ .

Besides the eigenvector convergence, we can examine the marginal posterior

$$\Pi(\mathcal{V} \mid \theta, y) \propto \Pi_0(K, V_1, \dots, V_K) \left\{ \prod_{k=1}^K \left[ \sum_{i \in V_k} r(y_i) \right] \right\} \prod_{k=1}^K \left\{ n_k^{-1} \prod_{h=2}^{n_k} \lambda_{(h)}(L_k) \right\},$$

where  $L_k$  is the unnormalized Laplacian matrix associated with matrix  $\{A_{i,j}\}_{i \in V_k, j \in V_k}$ . Imagine that if we put all indices in one partition  $V_1 = (1, \dots, n)$ , then  $\Pi(\mathcal{V} \mid \theta, y)$  would be very small due to those close-to-zero eigenvalues. Applying this deduction recursively on subsets of data, it is not hard to see that a high-valued  $\Pi(\mathcal{V} \mid \theta, y)$  would correspond to a partition, wherein each  $V_k$  has  $\lambda_{(h)}(L_k)$  away from 0 for any  $h \geq 2$ .

## 4.2 Consistent Clustering of Separable Sets

We show that clustering consistency is possible, under some separability assumptions when the data-generating distribution follows a forest process. Specifically, we establish posterior ratio consistency, as the ratio between the maximum posterior probability assigned to other possible clustering assignments to the posterior probability assigned to the true clustering assignments converges to zero almost surely under the true model (Cao et al., 2019).

To formalize the above, we denote the true cluster label for generating  $y_i$  by  $c_i^0$  (subject to label permutation among clusters), and we define the enclosing region for all possible  $y_i : c_i^0 = k$  as  $R_k^0$  for  $k = 1, \dots, K_0$  for some true finite  $K_0$ . And we refer to  $R^0 = (R_1^0, \dots, R_{K_0}^0)$  as the “null partition”. By separability, we mean the scenario that  $(R_1^0, \dots, R_{K_0}^0)$  are disjoint and there is a lower-bounded distance between each pair of sets. As alternatives, regions  $R = (R_1, \dots, R_K)$  could be induced by  $\{c_1, \dots, c_n\}$  from the posterior estimate of  $\mathcal{T}$ . For simplicity, we assume the scale parameter in  $f$  is known and all equal  $\sigma_{i,j} = \sigma^{0,n}$ .

Number of clusters is known. We first start with a simple case when we have fixed  $K = K_0$ . For regularities, we consider data as supported in a compact region  $\mathcal{X}$ , and satisfying the following assumptions:

- (A1, diminishing scale)  $\sigma^{0,n} = C'(1/\log n)^{1+\iota}$  for some  $\iota > 0$  and  $C' > 0$ .
- (A2, minimum separation)  $\inf_{x \in R_k^0, y \in R_{k'}^0} \|x - y\|_2 > M_n$ , for all  $k \neq k'$  with some positive constant  $M_n > 0$  such that  $M_n^2/\sigma^{0,n} = 8\tilde{m}_0 \log(n)$  for all  $(i, j)$  and is known for some constant  $\tilde{m}_0 > p/2 + 2$ .
- (A3, near-flatness of root density) For any  $n$ ,  $\epsilon_1 < r(y) < \epsilon_2$  for all  $y \in \mathcal{X}$ .

Under the null partition,  $\Pi(\mathcal{T}|y)$  is maximized at  $\mathcal{T} = \mathcal{T}_{\text{MST}, R^0}$ , which contains  $K_0$  trees with each  $T_k$  being the minimum spanning tree (denoted by subscript “MST”) within

region  $R_k^0$ . Similarly, for any alternative  $R$ ,  $\Pi(\mathcal{T}|y)$  is maximized at the  $\mathcal{T} = \mathcal{T}_{MST,R}$ .

**Theorem 2** *Under (A1,A2,A3), we have  $\Pi(\mathcal{T}_{MST,R}|y)/\Pi(\mathcal{T}_{MST,R^0}|y) \rightarrow 0$  almost surely, unless  $R_i^0 \subseteq R_{\xi(i)}$  for some permutation map  $\xi(\cdot)$ .*

Number of clusters is unknown: Next, we relax the condition by having a  $K$  not necessarily equal to  $K_0$ . We show the consistency in two parts for 1)  $K < K_0$ , and 2)  $K > K_0$  separately. In order to show posterior ratio consistency in the second part, we need some finer control on  $r(y)$ :

- (A3') The root density satisfies  $\tilde{m}_1 e^{-M/2\sigma^{0,n}} \leq r(y) \leq \tilde{m}_2 e^{-M/2\sigma^{0,n}}$  for some  $\tilde{m}_1 < \tilde{m}_2$ .

In this assumption, we essentially assume the root distribution to be flatter with a larger  $n$ . Then we have the following results.

**Theorem 3** *1) If  $K < K_0$ , under the assumptions (A1,A2,A3), we have*

*$\Pi(\mathcal{T}_{MST,R}|y)/\Pi(\mathcal{T}_{MST,R^0}|y) \rightarrow 0$  almost surely.*

*2) If  $K > K_0$ , under the assumptions (A1,A2,A3'), we have  $\Pi(\mathcal{T}_{MST,R}|y)/\Pi(\mathcal{T}_{MST,R^0}|y) \rightarrow 0$  almost surely.*

The above results show posterior ratio consistency. Furthermore, when the true of clusters is known, the ratio consistency result can be further extended to show clustering consistency, which is proved in the Supplementary Materials S3.

## 5 Numerical Experiments

### 5.1 Clustering Near-Manifold Data

To illustrate the capability of uncertainty quantification, we carry out clustering tasks on those near-manifold data commonly used for benchmarking clustering algorithms.

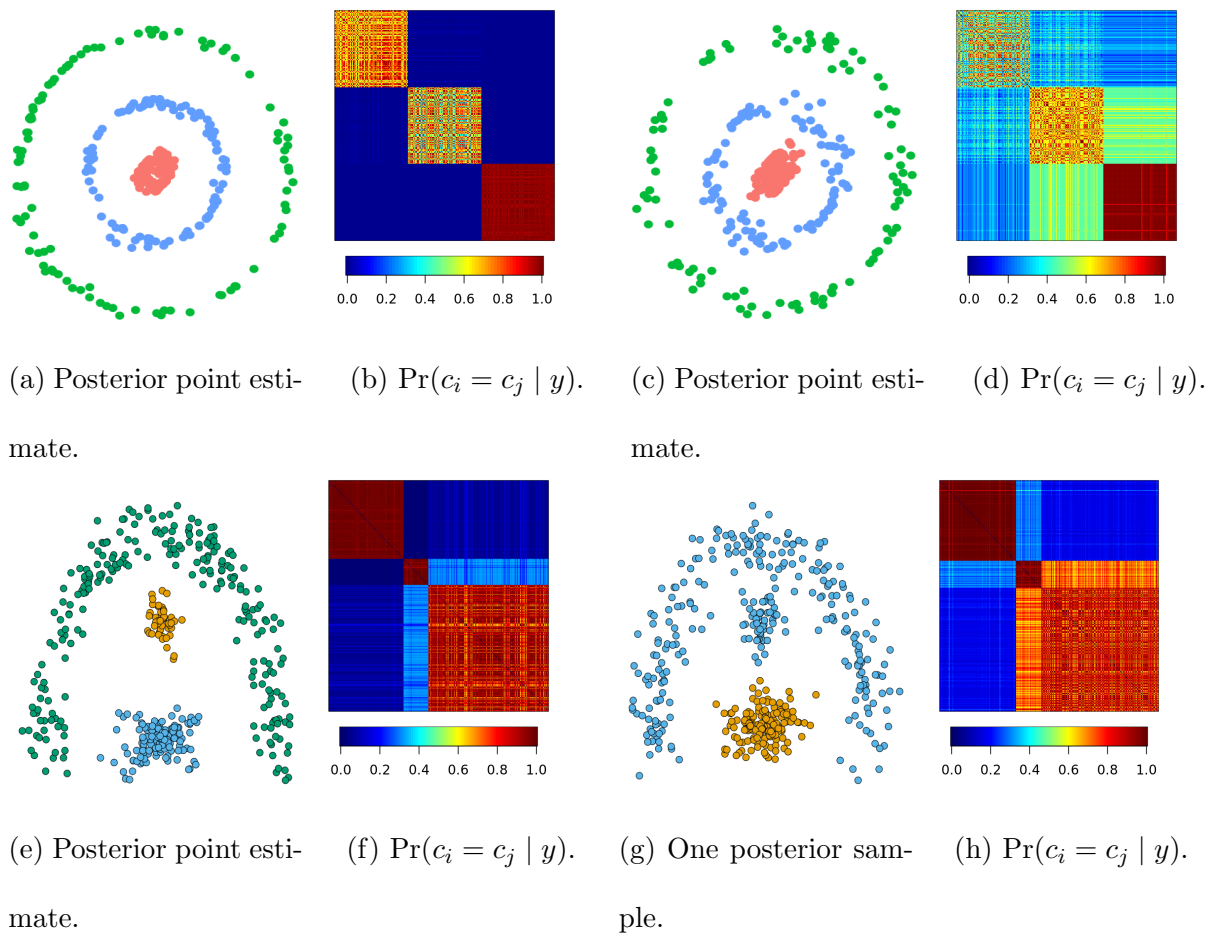


Figure 3: Uncertainty quantification in clustering data generated near three manifolds. When data are close to the manifolds (Panels a,e), there is very little uncertainty on clustering in low  $\Pr(c_i = c_j | j)$  between points from different clusters (Panels b,f). As data deviate more from the manifolds (Panel c,g), the uncertainty increases (Panels d,h). And in Panel g, the point estimate shows a two-cluster partitioning, while there is about 20% of probability for three-cluster partitioning.

In the first simulation, we start with 300 points drawn from three rings of radii 0.2, 1 and 2, with 100 points from each ring. Then we add some Gaussian noise to each point to create a coordinate near a ring manifold. We present two experiments, one with noises from  $N(0, 0.05^2 I_2)$ , and one with noises  $N(0, 0.1^2 I_2)$ . As shown in Figure 3, when these data are well separated (Panel a, showing Posterior point estimate), there is very little uncertainty



on the clustering (Panel b), with the posterior co-assignment  $\Pr(c_i = c_j | y)$  close to zero for any two data points near different rings. As noises increase, these data become more difficult to separate. There is a considerable amount of uncertainty for those red and blue points: these two sets of points are assigned into one cluster with a probability close to 40% (Panel d). We conduct another simulation based on an arc manifold and two point clouds (Panels e-h), and find similar results. Additional experiments are described in the Supplementary Materials S4.2.

## 5.2 Uncertainty Quantification for Data from Mixture Model

In the Supplementary Materials S4.1 and S4.3, we present some uncertainty quantification results, for clustering data that are from mixture models. We compare the estimates with the ones from Gaussian mixture models, which could correspond to correctly/erroneously specified component distribution. Empirically, we find that the uncertainty estimates on  $\Pr(c_i = c_j | y)$  and  $\Pr(K | y)$  from the forest model are close to the ones based on the true data-generating distribution; whereas the Gaussian mixture models suffer from sensitivity in model specification, especially when  $K$  is not known.

# 6 Application: Clustering in Multi-subject Functional Magnetic Resonance Imaging Data

In this application, we conduct a neuroscience study for finding connected brain regions under a varying degree of impact from Alzheimer’s disease. The source dataset is resting-state functional magnetic resonance imaging (rs-fMRI) scan data, collected from  $S = 166$  subjects at different stages of Alzheimer’s disease. Each subject has scans over  $n = 116$  regions of interest using the Automated Anatomical Labeling (AAL) atlas (Rolls et al., 2020; Shi et al., 2021) and over  $p = 120$  time points. We denote the observation for the

sth subject in the  $i$ th region by  $y_i^{(s)} \in \mathbb{R}^p$ .

The rs-fMRI data are known for their high variability, often characterized by a low intraclass correlation coefficient (ICC),  $(1 - \hat{\sigma}_{\text{within-group}}^2 / \hat{\sigma}_{\text{total}}^2)$ , as the estimate for the proportion of total variance that can be attributed to variability between groups (Noble et al., 2021). Therefore, our goal is to use the multi-view clustering to divide the regions of interest for each subject, while improving our understanding of the source of high variability.

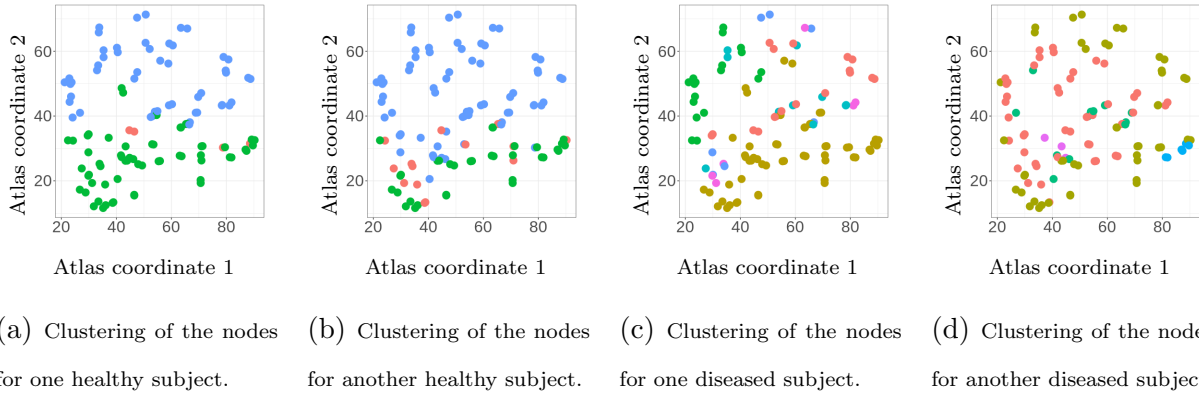


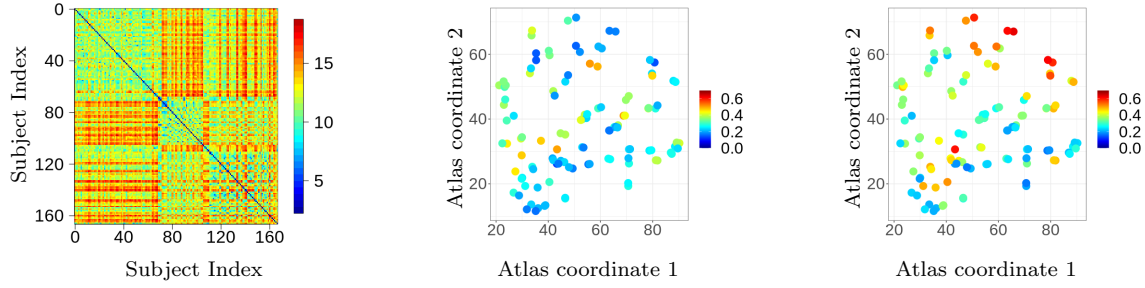
Figure 4: Results of brain region clustering (lateral view) for four subjects taken from the healthy and diseased groups. The multi-view clustering model allows subjects to have similar partition structures on a subset of nodes, while having subtle differences on the others (Panels a and b, Panels c and d). At the same time, the healthy subjects show less degree of variability in the brain clustering than the diseased subjects.

We fit the multi-view clustering model to the data, by running MCMC for 5,000 iterations and discarding the first 2,500 as burn-in. As shown in Figure 4, the hierarchical Dirichlet distribution on the latent coordinates induces similarity between the clustering of brain regions among subjects on a subset of nodes, while showing subtle differences on the other nodes. On the other hand, some major differences can be seen in the clusterings between the healthy and diseased subjects. Using the latent coordinates (at the posterior mean), we quantify the distances between  $z^{(s)}$  and  $z^{(s')}$  for each pair of subjects  $s \neq s'$ . As

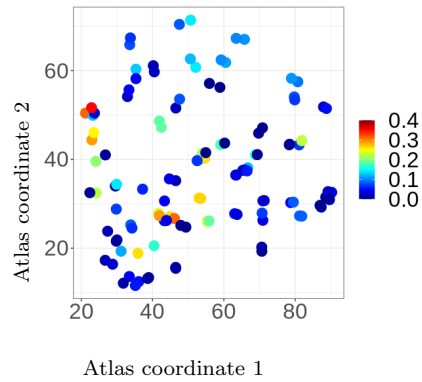
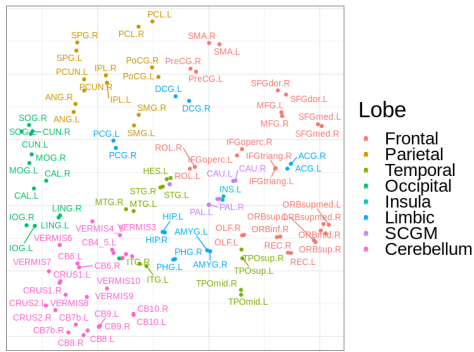
shown in Figure 5(a), there is a clear two-group structure in the pairwise distance matrix formed by  $\|z^{(s)} - z^{(s')}\|_F$ , and the separation corresponds to the first 64 subjects being healthy (denoted by  $s \in g_1$ ) and the latter 102 being diseased (denoted by  $s \in g_2$ ).

Next, we compute the within-group variances for these two groups, using  $\sum_{s \in g_l} \|z_i^{(s)} - (\sum_{s \in g_l} z_i^{(s)} / |g_l|)\|_F^2 / |g_l|$  for  $l = 1$  and  $2$ , and plot the variance over each region of interest  $i$  on the spatial coordinate of the atlas. Figure 5(b) and (c) show that, although both groups show some degree of variability, the diseased group shows clearly higher variances in some regions of the brain. Specifically, the paracentral lobule (PCL) and superior parietal gyrus (SPG), dorsolateral superior frontal gyrus (SFGdor), and supplementary motor area (SMA) in the frontal lobe show the highest amount of variability. Indeed, those regions are also associated with very low ICC scores [Figure 5(e)] calculated based on the variance of  $z_i^{(s)}$ , with pooled estimates  $\hat{\sigma}_{\text{total},i}^2 = \sum_s \|z_i^{(s)} - (\sum_s z_i^{(s)} / S)\|_F^2 / S$  and  $\hat{\sigma}_{\text{within-group},i}^2 = \sum_{l=1}^2 \sum_{s \in g_l} \|z_i^{(s)} - (\sum_{s \in g_l} z_i^{(s)} / |g_l|)\|_F^2 / S$ . On the other hand, some regions such as the hippocampus (HIP), parahippocampal gyrus (PHG), and superior occipital gyrus (SOG) show relatively lower variances within each group, hence higher ICC scores.

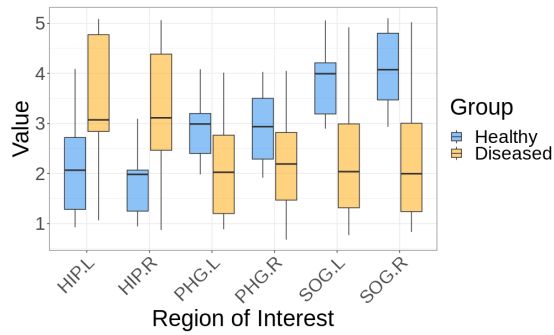
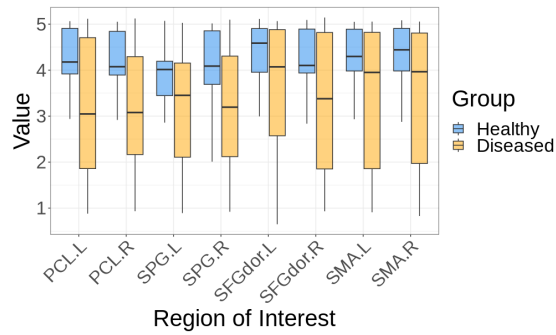
To show more details on the heterogeneity, we plot the latent coordinates associated with those ROIs using boxplots. Since each  $z_i^{(s)}$  is in two-dimensional space, we plot the linear transform  $\tilde{z}_i^{(s)} = z_{i,1}^{(s)} + z_{i,2}^{(s)}$ . Interestingly, those 8 ROIs with high variability still seem quite informative for distinguishing the two groups (Figure 5(f)). To verify, we concatenate those latent coordinates and form an  $S \times 16$  matrix, and fit them in a logistic regression model for classifying the healthy versus diseased states. The Area Under the Curve (AUC) of the Receiver Operating Characteristic is 86.6%. On the other hand, when we fit the 6 ROIs with low variability in logistic regression, the AUC increases to 96.1%.



(a) Pairwise distance of the latent coordinates  $\|z^{(s)} - z^{(s')}\|_F$  between subjects, the first 64 subjects are healthy and the latter 102 are diseased. (b) Within-group variances of  $z_i^{(\cdot)}$  for subjects in the healthy group, plotted over the automated anatomical labeling atlas. (c) Within-group variances of  $z_i^{(\cdot)}$  for subjects in the diseased group, plotted over the automated anatomical labeling atlas.



(d) The regions of interest (ROIs) colored by the associated lobe names, under the automated anatomical labeling atlas. (e) Intraclass correlation coefficients for the regions of interest  $(1 - \sigma_{\text{within-group},i}^2 / \sigma_{\text{total},i}^2)$ .



(f) Boxplot visualization of the latent coordinates for the regions with high variability in the diseased group. (g) Boxplot visualization of the latent coordinates for the regions with low variability in the diseased group.

Figure 5: Using the latent coordinates to characterize the heterogeneity within the subjects.

An explanation for the above results is that Alzheimer’s disease does different degrees of damage in the frontal and parietal lobes (see the two distinct clusterings in Figure 4 (c) and (d)), and the severity of the damage can vary from person to person. On the other hand, the hippocampus region (HIP and PHG), important for memory consolidation, is known to be commonly affected by Alzheimer’s disease (Braak and Braak, 1991; Klimova et al., 2015), which explains the low heterogeneity in the diseased group. Further, to our best knowledge, the high discriminability of the superior occipital gyrus (SOG) is a new quantitative finding, that could be meaningful for a further clinical study.

For validation, without using any group information, we concatenate those  $z_i^{(s)}$ ’s over all  $i = 1, \dots, 116$  and form an  $S \times 232$  matrix and use lasso logistic regression to classify the two groups. When 12 predictors are selected (as a similar-size model to the one above using 6 ROIs), the AUC is 96.4%. Since  $z_i^{(s)}$ ’s are obtained in an unsupervised way, this validation result shows that the multi-view clustering model produces meaningful representation for the nodes in this Alzheimer’s disease data. We provide further details on the clusterings, including the number of clusters, and the posterior co-assignment probability matrices in the Supplementary Materials S4.5.

## 7 Discussion

In this article, we present our discovery of a probabilistic model for popular spectral clustering algorithms. This enables straightforward uncertainty quantification and model-based extensions through the Bayesian framework. There are several directions worth exploring. First, our consistency theory is conducted under the condition of separable sets, similar to Ascolani et al. (2022). For general cases with non-separable sets, clustering consistency (especially on estimating  $K$ ) is challenging to achieve; to our best knowledge, existing consistency theory only applies to data generated independently from a mixture model (Miller

and Harrison, 2018; Zeng et al., 2020). For data generated dependently via a graph, this is still an unsolved problem. Second, in all of our forest models, we have been careful in choosing densities with tractable normalizing constants. One could relax this constraint by using densities  $f(y_i | y_j, \theta) = \alpha_f g_f(y_i | y_j; \theta)$  and  $r(y_i; \theta) = \alpha_r g_r(y_i; \theta)$ , with  $g$  some similarity function, and  $(\alpha_f, \alpha_r)$  potentially intractable. In these cases, the forest posterior becomes  $\Pi(\mathcal{T} | \cdot) \propto (\lambda \alpha_r / \alpha_f)^K \prod_{(0,i) \in \mathcal{T}} g_r(y_i; \theta) \prod_{(i,j) \in \mathcal{T}} g_r(y_i | y_j; \theta)$ . Therefore, one could choose an appropriate  $\tilde{\lambda} = \lambda \alpha_r / \alpha_f$  (equivalent to choosing some value of  $\lambda$ ), without knowing the value of  $\alpha_f$  or  $\alpha_r$ ; nevertheless, how to calibrate  $\tilde{\lambda}$  still requires further study. Third, a related idea is the Dirichlet Diffusion Tree (Neal, 2003), which considers a particle starting at the origin, following the path of previous particles, and diverging at a random time. The data are collected as the locations of particles at the end of a time period. Compared to the forest process, the diffusion tree process has the conditional likelihood given the tree invariant to the ordering of the data index, which is a stronger property compared to the marginal exchangeability of the data points. Therefore, it is interesting to further explore the relationship between those two processes.

## References

- Aldous, D. J. (1990). The Random Walk Construction of Uniform Spanning Trees and Uniform Labelled Trees. *SIAM Journal on Discrete Mathematics* 3(4), 450–465.
- Ascolani, F., A. Lijoi, G. Rebaudo, and G. Zanella (2022). Clustering Consistency With Dirichlet Process Mixtures. *arXiv preprint arXiv:2205.12924*.
- Aßmann, C., J. Boysen-Hogrefe, and M. Pape (2016). Bayesian Analysis of Static and Dynamic Factor Models: An Ex-Post Approach Towards the Rotation Problem. *Journal of Econometrics* 192(1), 190–206.
- Banerjee, S., R. Akbani, and V. Baladandayuthapani (2015). Bayesian Nonparametric Graph Clustering. *arXiv preprint arXiv:1509.07535*.
- Barry, D. and J. A. Hartigan (1993). A Bayesian Analysis for Change Point Problems. *Journal of the American Statistical Association* 88(421), 309–319.

- Bergé, L., C. Bouveyron, and S. Girard (2012). HDclassif: An R Package for Model-Based Clustering and Discriminant Analysis of High-Dimensional Data. *Journal of Statistical Software* 46(6), 1–29.
- Blackwell, D. and J. B. MacQueen (1973). Ferguson Distributions via Pólya Urn Schemes. *The Annals of Statistics* 1(2), 353–355.
- Blei, D. M. and P. I. Frazier (2011). Distance Dependent Chinese Restaurant Processes. *Journal of Machine Learning Research* 12(8).
- Boykov, Y., O. Veksler, and R. Zabih (2001). Fast Approximate Energy Minimization via Graph Cuts. *IEEE Transactions on pattern analysis and machine intelligence* 23(11), 1222–1239.
- Braak, H. and E. Braak (1991). Neuropathological Staging of Alzheimer-Related Changes. *Acta Neuropathologica* 82(4), 239–259.
- Broder, A. Z. (1989). Generating Random Spanning Trees. In *Annual Symposium on Foundations of Computer Science*, Volume 89, pp. 442–447.
- Brown, P. J. and J. E. Griffin (2010). Inference With Normal-Gamma Prior Distributions in Regression Problems. *Bayesian Analysis* 5(1), 171 – 188.
- Byrne, S. and A. P. Dawid (2015). Structural Markov Graph Laws for Bayesian Model Uncertainty. *The Annals of Statistics* 43(4), 1647–1681.
- Cai, D., T. Campbell, and T. Broderick (2021). Finite Mixture Models Do Not Reliably Learn the Number of Components. In *International Conference on Machine Learning*, pp. 1158–1169. PMLR.
- Cao, X., K. Khare, and M. Ghosh (2019). Posterior Graph Selection and Estimation Consistency for High-Dimensional Bayesian DAG Models. *The Annals of Statistics* 47(1), 319–348.
- Chaiken, S. and D. J. Kleitman (1978). Matrix Tree Theorems. *Journal of Combinatorial Theory, Series A* 24(3), 377–381.
- Chandra, N. K., A. Canale, and D. B. Dunson (2020). Escaping the Curse of Dimensionality in Bayesian Model Based Clustering. *arXiv preprint arXiv:2006.02700*.
- Chi, Y., X. Song, D. Zhou, K. Hino, and B. L. Tseng (2007). Evolutionary Spectral Clustering by Incorporating Temporal Smoothness. In *Proceedings of the 13th ACM SIGKDD international conference on Knowledge discovery and data mining*, pp. 153–162.
- Coretto, P. and C. Hennig (2016). Robust Improper Maximum Likelihood: Tuning, Computation, and a Comparison With Other Methods for Robust Gaussian Clustering. *Journal of the American Statistical Association* 111(516), 1648–1659.
- Crowley, E. M. (1997). Product Partition Models for Normal Means. *Journal of the American Statistical Association* 92(437), 192–198.

- Dahl, D. B., D. J. Johnson, and P. Müller (2022). Search Algorithms and Loss Functions for Bayesian Clustering. *Journal of Computational and Graphical Statistics* 31(4), 1189–1201.
- DeBruine, Z. J., K. Melcher, and T. J. Triche Jr (2021). Fast and Robust Non-Negative Matrix Factorization for Single-Cell Experiments. *bioRxiv*, 2021–09.
- Diaconis, P. (1977). Finite Forms of de Finetti’s Theorem on Exchangeability. *Synthese* 36, 271–281.
- Duan, L. L. and D. B. Dunson (2021a). Bayesian Distance Clustering. *Journal of Machine Learning Research* 22, 1–27.
- Duan, L. L. and D. B. Dunson (2021b). Bayesian Spanning Tree: Estimating the Backbone of the Dependence Graph. *arXiv preprint arXiv:2106.16120*.
- Duan, L. L., G. Michailidis, and M. Ding (2019). Spiked Laplacian Graphs: Bayesian Community Detection in Heterogeneous Networks. *arXiv preprint arXiv:1910.02471*.
- Edwards, D., G. C. De Abreu, and R. Labouriau (2010). Selecting High-Dimensional Mixed Graphical Models Using Minimal AIC or BIC Forests. *BMC Bioinformatics* 11(1), 1–13.
- Ester, M., H.-P. Kriegel, J. Sander, and X. Xu (1996). A Density-Based Algorithm for Discovering Clusters in Large Spatial Databases with Noise. In *Proceedings of the Second International Conference on Knowledge Discovery and Data Mining*, pp. 226–231. AAAI Press.
- Fraley, C. and A. E. Raftery (2002). Model-Based Clustering, Discriminant Analysis, and Density Estimation. *Journal of the American Statistical Association* 97(458), 611–631.
- Frey, B. J. and D. Dueck (2007). Clustering by Passing Messages Between Data Points. *Science* 315(5814), 972–976.
- Frühwirth-Schnatter, S. and S. Pyne (2010). Bayesian Inference for Finite Mixtures of Univariate and Multivariate Skew-Normal and Skew-t Distributions. *Biostatistics* 11(2), 317–336.
- Gelman, A. and D. B. Rubin (1992). Inference From Iterative Simulation Using Multiple Sequences. *Statistical Science*, 457–472.
- Geng, J., A. Bhattacharya, and D. Pati (2019). Probabilistic Community Detection With Unknown Number of Communities. *Journal of the American Statistical Association* 114(526), 893–905.
- Georghiades, A. S., P. N. Belhumeur, and D. J. Kriegman (2001). From Few to Many: Illumination Cone Models for Face Recognition Under Variable Lighting and Pose. *IEEE Transactions on Pattern Analysis and Machine Intelligence* 23(6), 643–660.
- Gower, J. C. and G. J. Ross (1969). Minimum Spanning Trees and Single Linkage Cluster Analysis. *Journal of the Royal Statistical Society: Series C (Applied Statistics)* 18(1), 54–64.



- Guha, S. and V. Baladandayuthapani (2016). A Nonparametric Bayesian Technique for High-Dimensional Regression. *Electronic Journal of Statistics* 10(2), 3374–3424.
- Han, X., X. Tong, and Y. Fan (2021). Eigen Selection in Spectral Clustering: A Theory-Guided Practice. *Journal of the American Statistical Association*, 1–13.
- Hartigan, J. A. (1981). Consistency of Single Linkage for High-Density Clusters. *Journal of the American Statistical Association* 76, 388–394.
- Hartigan, J. A. (1990). Partition Models. *Communications in Statistics-Theory and Methods* 19(8), 2745–2756.
- Horst, A. M., A. P. Hill, and K. B. Gorman (2020). palmerpenguins: Palmer Archipelago (Antarctica) Penguin Data. R package version 0.1.0.
- Karatzoglou, A., A. Smola, K. Hornik, and A. Zeileis (2004). Kernlab—An S4 Package for Kernel Methods in R. *Journal of Statistical Software* 11, 1–20.
- Klimova, B., P. Maresova, M. Valis, J. Hort, and K. Kuca (2015). Alzheimer’s Disease and Language Impairments: Social Intervention and Medical Treatment. *Clinical interventions in aging*, 1401–1408.
- Kosmidis, I. and D. Karlis (2016). Model-Based Clustering Using Copulas With Applications. *Statistics and Computing* 26(5), 1079–1099.
- Kuhn, H. W. (1955). The Hungarian Method for the Assignment Problem. *Naval Research Logistics Quarterly* 2(1-2), 83–97.
- Kumar, A., P. Rai, and H. Daume (2011). Co-regularized Multi-view Spectral Clustering. In J. Shawe-Taylor, R. Zemel, P. Bartlett, F. Pereira, and K. Weinberger (Eds.), *Advances in Neural Information Processing Systems*, Volume 24. Curran Associates, Inc.
- Lee, S. X. and G. J. McLachlan (2016). Finite Mixtures of Canonical Fundamental Skew t-Distributions. *Statistics and computing* 26(3), 573–589.
- Lei, J. and K. Z. Lin (2022). Bias-Adjusted Spectral Clustering in Multi-Layer Stochastic Block Models. *Journal of the American Statistical Association*, 1–13.
- Lei, J. and A. Rinaldo (2015). Consistency of Spectral Clustering in Stochastic Block Models. *The Annals of Statistics* 43(1), 215–237.
- Lewis, J. R., S. N. MacEachern, and Y. Lee (2021). Bayesian Restricted Likelihood Methods: Conditioning on Insufficient Statistics in Bayesian Regression. *Bayesian Analysis* 16(4), 1393–1462.
- Loftsgaarden, D. O. and C. P. Quesenberry (1965). A Nonparametric Estimate of a Multivariate Density Function. *The Annals of Mathematical Statistics* 36(3), 1049–1051.
- Luo, Z., H. Sang, and B. Mallick (2021). A Bayesian Contiguous Partitioning Method for Learning Clustered Latent Variables. *Journal of Machine Learning Research* 22.

- MacQueen, J. (1967). Classification and Analysis of Multivariate Observations. In *5th Berkeley Symp. Math. Statist. Probability*, pp. 281–297.
- Malsiner-Walli, G., S. Frühwirth-Schnatter, and B. Grün (2017). Identifying Mixtures of Mixtures Using Bayesian Estimation. *Journal of Computational and Graphical Statistics* 26(2), 285–295.
- McDaid, A. F., T. B. Murphy, N. Friel, and N. J. Hurley (2013). Improved Bayesian Inference for the Stochastic Block Model With Application to Large Networks. *Computational Statistics & Data Analysis* 60, 12–31.
- Medvedovic, M. and S. Sivaganesan (2002). Bayesian Infinite Mixture Model Based Clustering of Gene Expression Profiles. *Bioinformatics* 18(9), 1194–1206.
- Meilă, M. and T. Jaakkola (2006). Tractable Bayesian Learning of Tree Belief Networks. *Statistics and Computing* 16(1), 77–92.
- Meila, M. and M. I. Jordan (2000). Learning With Mixtures of Trees. *Journal of Machine Learning Research* 1(Oct), 1–48.
- Miller, J. W. (2019). An Elementary Derivation of the Chinese Restaurant Process From Sethuraman’s Stick-Breaking Process. *Statistics & Probability Letters* 146, 112–117.
- Miller, J. W. and D. B. Dunson (2018). Robust Bayesian Inference via Coarsening. *Journal of the American Statistical Association* 114(527), 1113–1125.
- Miller, J. W. and M. T. Harrison (2018). Mixture Models With a Prior on the Number of Components. *Journal of the American Statistical Association* 113(521), 340–356.
- Molitor, J., M. Papatomas, M. Jerrett, and S. Richardson (2010). Bayesian Profile Regression With an Application to the National Survey of Children’s Health. *Biostatistics* 11(3), 484–498.
- Mosbah, M. and N. Saheb (1999). Non-Uniform Random Spanning Trees on Weighted Graphs. *Theoretical Computer Science* 218(2), 263–271.
- Müller, P. and F. Quintana (2010). Random Partition Models With Regression on Covariates. *Journal of Statistical Planning and Inference* 140(10), 2801–2808.
- Müller, P., F. Quintana, and G. L. Rosner (2011). A Product Partition Model With Regression on Covariates. *Journal of Computational and Graphical Statistics* 20(1), 260–278.
- Neal, R. M. (2003). Density Modeling and Clustering Using Dirichlet Diffusion Trees. *Bayesian Statistics* 7, 619–629.
- Ng, S.-K., G. J. McLachlan, K. Wang, L. Ben-Tovim Jones, and S.-W. Ng (2006). A Mixture Model With Random-Effects Components for Clustering Correlated Gene-Expression Profiles. *Bioinformatics* 22(14), 1745–1752.

- Noble, S., D. Scheinost, and R. T. Constable (2021). A Guide to the Measurement and Interpretation of fMRI Test-Retest Reliability. *Current Opinion in Behavioral Sciences* 40, 27–32.
- Nowicki, K. and T. A. B. Snijders (2001). Estimation and Prediction for Stochastic Block-structures. *Journal of the American Statistical Association* 96(455), 1077–1087.
- Ord, K. (1975). Estimation Methods for Models of Spatial Interaction. *Journal of the American Statistical Association* 70(349), 120–126.
- Paganin, S., A. H. Herring, A. F. Olshan, and D. B. Dunson (2021). Centered Partition Processes: Informative Priors for Clustering. *Bayesian Analysis* 16(1), 301–370.
- Park, J.-H. and D. B. Dunson (2010). Bayesian Generalized Product Partition Model. *Statistica Sinica*, 1203–1226.
- Petrone, S., M. Guindani, and A. E. Gelfand (2009). Hybrid Dirichlet mixture models for functional data. *Journal of the Royal Statistical Society: Series B (Statistical Methodology)* 71(4), 755–782.
- Pinelis, I. (2020). Exact Lower and Upper Bounds on the Incomplete Gamma Function. *arXiv preprint arXiv:2005.06384*.
- Prim, R. C. (1957). Shortest Connection Networks and Some Generalizations. *The Bell System Technical Journal* 36(6), 1389–1401.
- Quintana, F. A. and P. L. Iglesias (2003). Bayesian Clustering and Product Partition Models. *Journal of the Royal Statistical Society: Series B (Statistical Methodology)* 65(2), 557–574.
- Rasmussen, C., J. Bernard, Z. Ghahramani, and D. L. Wild (2008). Modeling and Visualizing Uncertainty in Gene Expression Clusters Using Dirichlet Process Mixtures. *IEEE/ACM Transactions on Computational Biology and Bioinformatics* 6(4), 615–628.
- Ren, L., L. Du, L. Carin, and D. B. Dunson (2011). Logistic Stick-Breaking Process. *Journal of Machine Learning Research* 12(1).
- Rigon, T., A. H. Herring, and D. B. Dunson (2020). A Generalized Bayes Framework for Probabilistic Clustering. *arXiv preprint arXiv:2006.05451*.
- Rodríguez, C. E. and S. G. Walker (2014). Univariate Bayesian Nonparametric Mixture Modeling With Unimodal Kernels. *Statistics and Computing* 24(1), 35–49.
- Rohe, K., S. Chatterjee, and B. Yu (2011). Spectral Clustering and the High-Dimensional Stochastic Blockmodel. *The Annals of Statistics* 39(4), 1878–1915.
- Rolls, E. T., C.-C. Huang, C.-P. Lin, J. Feng, and M. Joliot (2020). Automated Anatomical Labelling Atlas 3. *Neuroimage* 206, 116189.
- Ross, G. J. and D. Markwick (2018). *dirichletprocess*: An R Package for Fitting Complex Bayesian Nonparametric Models.

- Schild, A. (2018). An Almost-Linear Time Algorithm for Uniform Random Spanning Tree Generation. In *Proceedings of the 50th Annual ACM SIGACT Symposium on Theory of Computing*, pp. 214–227.
- Scrucca, L., M. Fop, T. B. Murphy, and A. E. Raftery (2016). MCLUST 5: Clustering, Classification and Density Estimation Using Gaussian Finite Mixture Models. *The R Journal* 8(1), 289.
- Shi, D., H. Zhang, S. Wang, G. Wang, and K. Ren (2021). Application of Functional Magnetic Resonance Imaging in the Diagnosis of Parkinson’s Disease: A Histogram Analysis. *Frontiers in Aging Neuroscience* 13, 624731.
- Shi, T., M. Belkin, and B. Yu (2009). Data Spectroscopy: Eigenspaces of Convolution Operators and Clustering. *The Annals of Statistics*, 3960–3984.
- Snijders, T. A. and K. Nowicki (1997). Estimation and Prediction for Stochastic Block-models for Graphs With Latent Block Structure. *Journal of classification* 14(1), 75–100.
- Socher, R., A. Maas, and C. Manning (2011). Spectral Chinese Restaurant Processes: Non-parametric Clustering Based on Similarities. In *Proceedings of the Fourteenth International Conference on Artificial Intelligence and Statistics*, pp. 698–706. JMLR Workshop and Conference Proceedings.
- Teh, Y. W., M. I. Jordan, M. J. Beal, and D. M. Blei (2006). Hierarchical dirichlet processes. *Journal of the American Statistical Association* 101(476), 1566–1581.
- Vidal, R. (2011). Subspace Clustering. *IEEE Signal Processing Magazine* 28(2), 52–68.
- Von Luxburg, U. (2007). A Tutorial on Spectral Clustering. *Statistics and Computing* 17(4), 395–416.
- Wade, S. and Z. Ghahramani (2018). Bayesian Cluster Analysis: Point Estimation and Credible Balls. *Bayesian Analysis* 13(2), 559–626.
- Wu, S., X. Feng, and W. Zhou (2014). Spectral Clustering of High-Dimensional Data Exploiting Sparse Representation Vectors. *Neurocomputing* 135, 229–239.
- Yu, Y., T. Wang, and R. J. Samworth (2015). A Useful Variant of the Davis–Kahan Theorem for Statisticians. *Biometrika* 102(2), 315–323.
- Zelnik-Manor, L. and P. Perona (2005). Self-Tuning Spectral Clustering. In *Advances in Neural Information Processing Systems*, Volume 17.
- Zeng, C., J. W. Miller, and L. L. Duan (2020). Quasi-Bernoulli Stick-Breaking: Infinite Mixture With Cluster Consistency. *arXiv preprint arXiv:2008.09938*.

# S1 Model-based Extensions to Forest Model

## S1.1 Extension to High-dimensional Clustering Model

For clustering high dimensional data, good performances have been demonstrated through finding a low-dimensional sparse representation  $z_i$  for each  $y_i$  (Vidal, 2011; Wu et al., 2014), and then clustering  $z_i$  instead of  $y_i$ . To briefly review the idea, for high-dimensional data, a useful assumption is that  $y_i \in \mathbb{R}^p$  can be “reconstructed” using a linear combination of a few other  $y_j$ ’s, that is,  $y_i \approx \sum_j w_{i,j} y_j$ , with  $w_{i,i} = 0$  and  $w_i = (w_{i,1}, \dots, w_{i,n})$  contains only a few non-zeros.

Although  $w_i$  is obtained as a vector of coefficients, it can be viewed as a low-dimensional *relative* coordinate, that can be used instead of the absolute coordinate  $y_i \in \mathbb{R}^p$ . The key idea is that if  $w_i$  and  $w_j$  are in different subspaces ( $w_i' w_j = 0$ ), then  $y_i$  and  $y_j$  are likely to be in different clusters. Using a similarity function defined on each pair  $(w_i, w_j)$ , one could obtain a similarity matrix and then apply the spectral clustering algorithm.

We now propose a generative distribution. We use  $W = [w_1', \dots, w_n']$  as the  $n \times n$  matrix with the  $i$ th row equal to  $w_i$ , and  $Y$  the  $n \times p$  data matrix. We include the reconstruction loss  $\|Y - WY\|_F^2$  (with  $\|\cdot\|_F$  the Frobenius norm) via a matrix Gaussian distribution:

$$Y \sim \text{Matrix-Gaussian}\{O, \sigma_y^2[(I_n - W)'(I_n - W)]^{-1}, I_p\}.$$

We note a link between this model and the spatial autoregressive (SAR) model (Ord, 1975), except that the neighborhood information  $W$  is not known. We view each  $w_i$  as a transform of another unit-norm vector  $z_i$  that satisfies  $\|z_i\|_2 = 1$  and  $\|z_i\|_0 = d$  (the number of non-zeros is  $d$ ) via

$$w_{i,k} = \alpha_i z_{i,k}, \text{ for } k \neq i, \quad w_{i,i} = 0, \quad z_{i,i} \in \mathbb{R},$$

with  $\alpha_i > 0$  some scale parameter, and  $z_{i,i}$  not necessarily zero. And we model  $(z_1, \dots, z_n)$  as from a forest model based on sparse von Mises–Fisher densities:

$$\begin{aligned} z_1, \dots, z_n &\sim \text{Forest Model}(\mathcal{T}), \\ f(z_i | z_j; \kappa) &\propto \exp(\kappa z_i' z_j) 1(z_i' z_j \neq 0) 1(\|z_i\|_2 = 1, \|z_i\|_0 = d), \\ r(z_i) &\propto 1(\|z_i\|_2 = 1, \|z_i\|_0 = d). \end{aligned}$$

The leaf  $f(z_i | z_j; \kappa)$  is supported in those  $(d-1)$ -dimensional unit spheres  $\mathcal{S}^{(d-1)} \subset \mathcal{S}^{(n-1)}$ , such that  $z_i$  and  $z_j$  are not in completely disjoint subspaces. The von Mises–Fisher density in a given  $\mathcal{S}^{(d-1)}$  has a tractable normalizing constant that depends on  $\kappa$  only. Further, with  $\|z_j\|_0 = d$ , we can easily tell the number of those  $\mathcal{S}^{(d-1)}$  with  $z_i : z_i' z_j \neq 0$  is equal to  $\binom{n}{d} - \binom{n-d}{d}$ . Similarly,  $r$  is a uniform density on all  $\mathcal{S}^{(d-1)} \subset \mathcal{S}^{(n-1)}$ . Therefore, both of the normalizing constants in  $f$  and  $r$  are available. We refer to the model for  $Y$  as a latent forest model.

One could further assign priors on  $\kappa$ ,  $\sigma_y^2$  and  $\alpha_i$ ’s, and develop a Gibbs sampling algorithm for posterior estimation. In this section, since our main focus is to demonstrate a high-dimensional model extension and compare the point estimates against a few other algorithms, we use a fast posterior approximation algorithm for the above model. Specifically, we first use the lasso algorithm to solve for a sparse  $\hat{W} = \arg \min_{W: w_{i,i}=0 \forall i} (1/2) \|Y -$

$WY\|_F^2 + \lambda\|W\|_1$  with  $\lambda = 1$ ; then for each  $\hat{w}_i$ , we take the top  $(d - 1)$  elements in magnitude, and set the other elements to zero. Then we replace  $w_{i,i}$  by 1 and normalize the vector to produce a unit 2-norm vector  $z_i$ . Conditioning on the transformed matrix  $\hat{Z}$  and  $\kappa$  fixed to 10, we sample the forest  $\mathcal{T}$  using the random-walk covering algorithm.

To assess the clustering performance, we use the image data from the Yale face database B (Georghiades et al., 2001). This dataset contains single light source images of 10 subjects. We take the ones corresponding to the forward-facing poses under 64 different illumination conditions (shown in Figure S.1). We resize each image to have  $48 \times 42$  pixels. We label those images by subject id from 1 to 10. Therefore, we have a clustering task with  $n = 640$  and  $p = 2,016$ .



(a) One subject under illumination condition 1.

(b) One subject under illumination condition 2.

(c) One subject under illumination condition 3.



(d) Another subject under illumination condition 1.

(e) Another subject under illumination condition 2.

(f) Another subject under illumination condition 3.

Figure S.1: a few sample photos from the Yale face database B (Georghiades et al., 2001).

We compare the performance against several popular clustering methods. To produce a point estimate, for the forest model on  $z_i$ 's, we apply spectral clustering with  $K = 10$  on the posterior co-assignment probability matrix (as described in the main text); for each of the other methods, we use  $K = 10$  as the specified parameter. To evaluate the clustering accuracy, we relabel the point estimate  $(c_1, \dots, c_n)$  using the Hungarian matching algorithm (Kuhn, 1955), so that the Hamming distance  $\text{dist}_h$  between  $(c_1, \dots, c_n)$  and the subject id's is minimized. Then the clustering accuracy is calculated as  $(n - \text{dist}_h)/n$ . As the accuracy

can be sensitive to the initialization of each algorithm, for a fair comparison, we repeat running each algorithm 20 times, and report the mean and the 95% confidence interval.

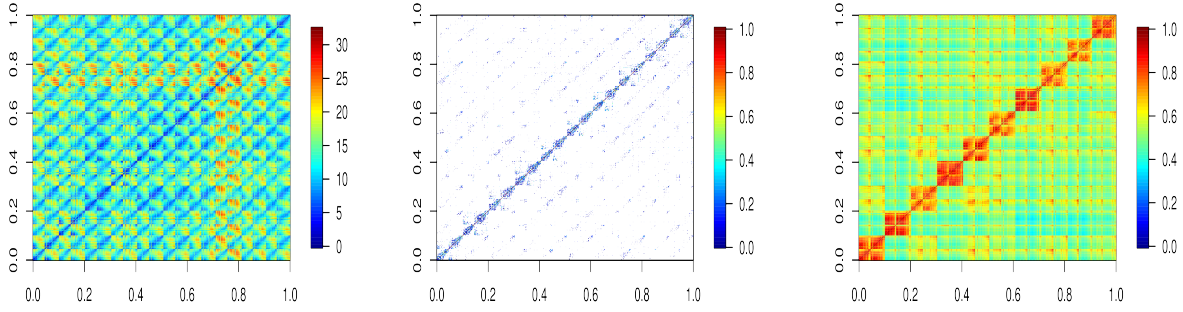
Method	K-means	Mclust (VII)	Mclust (VEI)	Mclust (EII)
Accuracy	0.18 (0.16, 0.21)	0.24 (0.24, 0.24)	0.26 (0.26, 0.26)	0.23 (0.23, 0.23)
Method	HDDC (AkjBkQkDk)	HDDC (AkjBQkDk)	SpecC on $e^{-\lambda_s \ y_i - y_j\ _2^2}$	SpecC on $y_i' y_j$
Accuracy	0.324	0.296	0.35 (0.25, 0.43)	0.30 (0.28, 0.34)
Method	K-means on $w_i$	SpecC on $(w_i' w_j)_+$	SpecC on $ w_{i,j}  +  w_{j,i} $	Forest on $z_i$
Accuracy	0.25 (0.18, 0.39)	0.64 (0.52, 0.69)	0.59 (0.46, 0.68)	0.82 (0.71, 0.93)

Table S.1: Clustering 640 face photos collected from 10 subjects.

Table S.1 shows the results. We use the K-means function from the native R library, the Mclust function in the MCLUST package (Scrucca et al., 2016) for various Gaussian mixture models, the hddc function in HDclassif (Bergé et al., 2012) package for Gaussian mixture models with near low-rank covariance matrices, and the specc function from the kernlab package (Karatzoglou et al., 2004) for the spectral clustering algorithm. For those spectral clustering algorithms, we use  $w_i$ 's as the sparse representation estimated from the lasso regression, without imposing a low-cardinality constraint. For the latent forest model, we use  $z_i$ 's with cardinality constraint at  $d = 4$ .

Clearly, for this high-dimensional dataset, clustering the sparse representation  $z_i$ 's (or  $w_i$ 's) instead of  $y_i$ 's has a significantly improved accuracy. Interestingly, we found that K-means on those  $w_i$ 's produce much worse results than all the spectral clustering algorithms. This suggests that forest models (as a generative model for spectral clustering) give a better fit to those  $w_i$ 's, compared to the Gaussian mixture models (as a generative model for K-means). Lastly, compared to the existing spectral clustering algorithms using similarity  $|w_{i,j}| + |w_{j,i}|$  (Vidal, 2011) or  $(w_i' w_j)_+$  (Wu et al., 2014), imposing a cardinality constraint seemed to further improve the signal that is helpful for clustering. To verify this, we also conducted spectral clustering using similarity  $(z_i' z_j)_+$  and obtained almost the same clustering accuracy as the one from the latent forest model.

As shown in Figure S.2, for this high-dimensional dataset, the pairwise Euclidean distance  $\|y_i - y_j\|_2$ 's are too noisy to be used for clustering, the inner product on the sparse  $z_i$  has much less noise, and the pairwise co-assignment probability matrix produces a very clear partition of 10 clusters.



(a) Euclidean distances between the latent  $y_i$ 's. (b)  $(z_i' z_j)$  between the latent  $z_i$ 's. (c)  $\Pr(c_i = c_j | y)$  from the latent forest model.

Figure S.2: Pairwise information between the observed  $y_i$ 's, and sparse latent  $z_i$ 's, and posterior co-assignment probability matrix in the latent forest model.

## S1.2 Extension to Covariate-dependent Forest Clustering

Following Müller et al. (2011), we now illustrate an extension where the clustering is dependent on external covariates  $x_i$ 's (each  $x_i$  is an  $m$ -dimension vector). Müller et al. (2011) proposed the following covariate-dependent product partition model (PPMx):

$$\Pi_0(V_1, \dots, V_K | K, x) \propto \prod_{k=1}^K C(V_k) G(\{x_i\}_{i \in V_k}),$$

where  $C$  and  $G$  together form a modified cohesion function, with  $G$  positive-valued and quantifying the overall similarity among those  $x_i : i \in V_k$ . To specify  $G$ , Müller et al. (2011) proposed to use

$$G(\{x_i\}_{i \in V_k}) = \int \left[ \prod_{i \in V_k} \tilde{g}_1(x_i; \xi_k) \right] \tilde{g}_2(\xi_k) d\xi_k$$

with  $\tilde{g}_1$  and  $\tilde{g}_2$  some probability density/mass functions with conjugacy, such as  $\tilde{g}_1$  as multivariate Gaussian  $N(\cdot | \mu_k, \Sigma_1)$  and  $\tilde{g}_2$  as Gaussian for  $N(\mu_k | 0, \Sigma_2)$ , with  $\Sigma_1$  and  $\Sigma_2$  some fixed parameters. Importantly, the purpose of  $G$  is to form a density-based cohesion function a priori, hence  $G$  is not interpreted as the generative distribution for  $x_i$ 's.

We note that the above  $G(\{x_i\}_{i \in V_k})$  effectively treats  $x_i : i \in V_k$  as conditionally independent. Now suppose there is a tree  $T_k$ , we can equivalently form a joint distribution by starting from a  $x_{k^*} \sim \tilde{g}_1(\cdot; \xi_k)$ , and then for any  $(i, j) \in T_k$ ,  $(x_j - x_i) \sim \tilde{g}_1^*(\cdot; \xi_k)$ , with  $\tilde{g}_1^*$  the transformed distribution on the difference. Therefore, we have a tree-based similarity function:

$$G(\{x_i\}_{i \in V_k}; T_k) = \int \left[ \tilde{g}_1(x_{k^*}; \xi_k) \prod_{(i,j) \in T_k} \tilde{g}_1^*(x_j - x_i; \xi_k) \right] \tilde{g}_2(\xi_k) d\xi_k.$$



In this section, we use Gaussian  $\tilde{g}_1$  and  $\tilde{g}_2$  as mentioned above. We have  $\tilde{g}_1^*$  as  $N(\cdot | 0, 2\Sigma_1)$ . After integration, we have

$$G(\{x_i\}_{i \in V_k}; T_k) = \prod_{(i,j) \in T_k} \underbrace{|2\pi(2\Sigma_1)|^{-1/2} \exp \left[ -(x_i - x_j)'(4\Sigma_1)^{-1}(x_i - x_j) \right]}_{f_0(x_i; x_j)} \times$$

$$\underbrace{|2\pi\Sigma_1\Sigma_2|^{-1/2} |\Sigma_1^{-1} + \Sigma_2^{-1}|^{-1/2} \exp \left[ -\frac{1}{2}x_{k^*}'\Sigma_1^{-1}x_{k^*} + \frac{1}{2}x_{k^*}'\Sigma_1^{-1}(\Sigma_1^{-1} + \Sigma_2^{-1})^{-1}\Sigma_1^{-1}x_{k^*} \right]}_{r_0(x_{k^*})},$$

where we use  $f_0$  and  $r_0$  to simplify notation. Therefore, we can achieve similar effects of PPMx, using an  $x$ -informative tree distribution:

$$\Pi(E_k | V_k)\Pi(k^* | E_k, V_k) = \frac{r_0(x_{k^*}) \prod_{(i,j) \in T_k} f_0(x_i; x_j)}{[\sum_{k \in V_k} r_0(x_k)] [\sum_{T'_k} \prod_{(i,j) \in T'_k} f_0(x_i; x_j)]},$$

$$\Pi_0(V_1, \dots, V_K, K) \propto \lambda^K \left\{ \prod_{k=1}^K [\sum_{k \in V_k} r_0(x_k)] [\sum_{T'_k} \prod_{(i,j) \in T'_k} f_0(x_i; x_j)] \right\}.$$

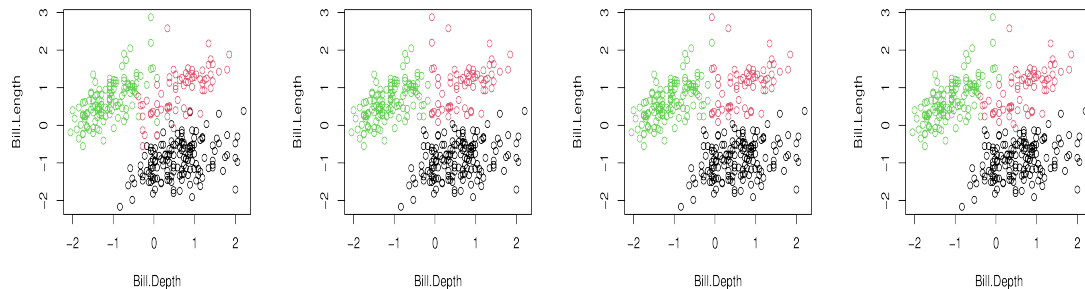
Note that if  $f_0(x_i; x_j) \propto 1$  for any  $(x_i, x_j)$ , and  $r_0(x_i) \propto 1$  for any  $x_i$ , then the above would be  $\Pi_0(V_1, \dots, V_K, K) = \lambda^K n_k^{n_k-1}$ , the same as the distribution we describe in the main text.

Compared to directly clustering  $(y_i, x_i)$  as the joint observation together, a strength of the above approach (and PPMx methods in general) is that a priori, we can directly control the influence from  $x_i$  to clustering, by adjusting the parameters in  $G$ . For example, we use  $\Sigma_1 = \Sigma_2 = \eta S_n$  with  $S_n$  the empirical covariance of  $x_i$ 's and  $\eta > 0$  an adjustable hyper-parameter. This leads to  $f_0(x_i; x_j) = |2\pi(2\Sigma_1)|^{-1/2} \exp[-(x_i - x_j)'(4\Sigma_1)^{-1}(x_i - x_j)]$  and  $r_0(x_{k^*}) = |2\pi(2\Sigma_1)|^{-1/2} \exp[-x_{k^*}'(4\Sigma_1)^{-1}x_{k^*}]$ . As  $\eta$  increases, the influence of  $x_i$  becomes weaker. Note that if we were to use  $x_i$  in a likelihood, we would not have such flexibility.

To illustrate this model, we use the Palmer Penguins dataset provided in the “palmer-penguins” package (Horst et al., 2020). To clarify, for such a clean dataset, existing approaches such as the Gaussian mixture model can also produce a similarly good accuracy; our goal here is to illustrate the high extensibility of the forest model via distribution specification.

We remove the duplicated data entries and have a sample of size  $n = 334$ . The dataset has observations about three species of Antarctic penguins, containing the length and depth measurements of each penguin’s bill (in mm). These two variables contain strong signals for distinguishing between species, and we denote each record of (length, depth) by  $y_i$ . In addition, the dataset also has measurements of flipper length (in mm) and body mass (in grams), and we denote each record by  $x_i$ .

As shown in Figure S.3, the forest model without using covariates correctly estimates most species labels. On the other hand, including the external information from  $x_i$  further increases the accuracy.



(a) Penguin data, colored by species. (b) Forest model estimate without using  $x_i$  as external covariates. (c) Forest model estimate using  $x_i$  as external covariates with  $\eta = 2$ . (d) Forest model estimate using  $x_i$  as external covariates with  $\eta = 1$ .

Figure S.3: Clustering the penguin data that contain records of bill length and depth. The forest model alone (Panel b) leads to a good estimate (accuracy 94.6%). Nevertheless, using external covariates (flipper length and body mass) gives more accurate estimates (Panel c: accuracy 95.8%, Panel d: accuracy 97.3%).

### S1.3 Algorithm for Estimating Multi-view Clustering

We use  $k_i^{(s)} \in \{1, \dots, \tilde{K}\}$  to denote the latent assignment  $k_i^{(s)} = l$ , for  $\eta_i^{(s)} = \eta_l^*$ . We use the following Gibbs sampling algorithm:

- Using  $L_{\mathcal{T}_{1:n,1:n}^{(s)}}$  to denote the Laplacian matrix of the forest graph without auxiliary node 0, we have

$$z^{(s)} \mid \eta^{(s)}, \mathcal{T}^{(s)} \sim \mathcal{N} \left\{ (L_{\mathcal{T}_{1:n,1:n}^{(s)}} / \rho + I / \sigma_z^2)^{-1} (\eta^{(s)} / \sigma_z^2), (L_{\mathcal{T}_{1:n,1:n}^{(s)}} / \rho + I / \sigma_z^2)^{-1} \right\}.$$

- Sample

$$\Pr(k_i^{(s)} = l \mid \cdot) \propto v_{i,l} \exp \left( -\frac{1}{2} \|z_j^{(s)} - \eta_l^*\|_2^2 / \sigma_z^2 \right).$$

- Sample  $v_i \sim \text{Dir}(\{1/\tilde{\kappa} + \sum_s 1(k_i^{(s)} = l)\}_{l=1, \dots, \tilde{\kappa}})$ .
- Sample  $\mathcal{T}^{(s)}$  and  $\theta^{(s)}$  for all  $s$ , according to the algorithm in Section 3.1 of the main text.

## S2 Proof of Theorems

### S2.1 Proof of Theorem 1

**Proof:** For ease of notation, in this proof, we use  $p = (n + 1)$ .

1. Obtain closed-form of the marginal connecting probability.

Since  $L$  correspond to a connected graph with weight  $A_{i,j} = \exp(W_{i,j})$  for  $i \neq j$  and  $A_{i,i} = 0$ , hence only has one eigenvalue equal to 0 and with eigenvector  $\vec{1}/\sqrt{p}$ , therefore we have:

$$p^{-1} \prod_{i=2}^{n+1} \lambda_{(i)}(L) = |L + J/p^2|,$$

where  $J = \vec{1}\vec{1}^\top$ . Let  $\tilde{L} = L + J/p^2$ , differentiating  $\log|\tilde{L}|$  with respect to  $W_{i,j}$  yields:

$$M_{i,j} = (\Omega_{i,i} + \Omega_{j,j} - 2\Omega_{i,j})A_{i,j},$$

where  $\Omega = \tilde{L}^{-1}$ , and  $M_{i,i} = 0$ .

## 2. Obtain $M$ as a perturbation form

Let  $L = \sum_{l=1}^p \lambda_l \psi_l \psi_l^\top$  be the eigendecomposition of  $L$ , and  $N = D^{-1/2}LD^{-1/2}$ . Note that,

$$\begin{aligned} M_{i,j} &= (\Omega_{i,i} + \Omega_{j,j} - 2\Omega_{i,j})A_{i,j} \\ &= (\Omega_{i,i} + \Omega_{j,j} - 2\Omega_{i,j})\{-L_{i,j}1(j \neq i)\} \\ &\stackrel{(a)}{=} \vec{b}_{i,j}^\top (L + J/p^2)^{-1} \vec{b}_{i,j} (-L_{i,j}) \\ &= D_i^{1/2} \vec{b}_{i,j}^\top (L + J/p^2)^{-1} \vec{b}_{i,j} D_j^{1/2} (-N_{i,j}) \end{aligned}$$

where (a) is due to  $\Omega_{i,i} + \Omega_{j,j} - 2\Omega_{i,j} = 0$  if  $1(j \neq i) = 0$ , hence  $1(k \neq i)$  can be omitted;  $\vec{b}_{i,j}$  is a binary vector with the  $i$ th element 1 and the  $k$ th element  $-1$ , and all other elements 0.

Let  $\alpha_{i,j} := D_i^{1/2} \vec{b}_{i,j}^\top (L + J/p^2)^{-1} \vec{b}_{i,j} D_j^{1/2}$  for  $i \neq j$ . Since  $N_{i,i} = 1$ , and  $x(I - N)$  has the same eigenvectors as  $N$  for any scalar  $x > 0$ , we see that  $M = -\alpha \circ (I - N)$  is an element-wise perturbation of  $x(I - N)$ . Therefore, our next task is to show  $\alpha$  is close to a simple  $xJ$  for some  $x > 0$ .

## 3. Bound the difference between the $K$ leading eigenvectors.

Slightly changing the above,

$$\begin{aligned} \alpha_{i,j} &= D_i^{1/2} \vec{b}_{i,j}^\top (L + J/p^2)^{-1} \vec{b}_{i,j} D_j^{1/2} \\ &= D_i^{1/2} \vec{b}_{i,j}^\top D^{-1/2} (N + D^{-1/2} J D^{-1/2} / p^2)^{-1} D^{-1/2} \vec{b}_{i,j} D_j^{1/2}. \end{aligned}$$

Using  $N = I - D^{-1/2}AD^{-1/2}$ , we have

$$\begin{aligned} (N + D^{-1/2} J D^{-1/2} / p^2)^{-1} &= \{I - D^{-1/2}(A - J/p^2)D^{-1/2}\}^{-1} \\ &\stackrel{(a)}{=} I + \sum_{k=1}^{\infty} \{D^{-1/2}(A - J/p^2)D^{-1/2}\}^k \\ &= I + E. \end{aligned}$$

where (a) uses the Neumann expansion, as  $E$  is not divergent:

$$E = D^{1/2}(L + J/p^2)^{-1}D^{1/2} - I = D^{1/2}\left(\sum_{l=2}^p \lambda_l^{-1} \psi_l \psi_l^\top + J\right)D^{1/2} - I,$$

as  $\lambda_2 > 0$ ,  $E$  is bounded element-wise for any  $D$  with finite-value elements. Further, note that  $D_i^{-1/2}(A_{i,j} - 1/p^2)D_j^{-1/2} \rightarrow 0$  and monotonically decreasing for fixed  $A_{i,j}$  and increasing

$D_i$  or  $D_j$ ; hence  $E$  is always bounded elementwise even as all  $D_i \rightarrow \infty$ . We denote the bound constant by  $\max_{i,j} |E_{i,j}| \leq \epsilon$ .

Combining the above,

$$\begin{aligned}\alpha_{i,j} &= D_i^{1/2} D_j^{1/2} \vec{b}_{i,j}^\top \left\{ D^{-1} + D^{-1/2} E D^{-1/2} \right\} \vec{b}_{i,j} \\ &= D_i^{1/2} D_j^{1/2} \left\{ (D_i^{-1} + D_j^{-1}) + (D_i^{-1} E_{i,i} + D_j^{-1} E_{j,j} - 2D_i^{-1/2} D_j^{-1/2} E_{i,j}) \right\}.\end{aligned}$$

Now we can bound the difference between  $M$  and  $x(I - N)$  minimized over  $x$ :

$$\begin{aligned}& \min_x \max_{i,j} | \{ (\alpha - xJ) \circ (I - N) \}_{i,j} | \\ &= \min_x \max_{i,j} | (\alpha_{i,j} - x) (D_i^{-1/2} D_j^{-1/2} A_{i,j}) | \\ &= \min_x \max_{i,j} \left| \left\{ (D_i^{-1} + D_j^{-1}) - x D_i^{-1/2} D_j^{-1/2} + (D_i^{-1} E_{i,i} + D_j^{-1} E_{j,j} - 2D_i^{-1/2} D_j^{-1/2} E_{i,j}) \right\} A_{i,j} \right| \\ &\leq \min_x \max_{i,j} \left| \left\{ (D_i^{-1} + D_j^{-1}) - x D_i^{-1/2} D_j^{-1/2} + (D_i^{-1} \epsilon + D_j^{-1} \epsilon + 2D_i^{-1/2} D_j^{-1/2} \epsilon) \right\} A_{i,j} \right| \\ &\stackrel{(a)}{\leq} \max_{i,j} \left\{ (1 + \epsilon) (D_i^{-1/2} - D_j^{-1/2})^2 A_{i,j} \right\},\end{aligned}$$

where (a) chooses  $x = 2(1 + \epsilon) + 2\epsilon$ .

Using Theorem 2 from Yu et al. (2015), there exists a orthonormal matrix  $R \in \mathbb{R}^{K \times K}$ , such that,

$$\|\Psi_{1:K} - \phi_{1:K} R\|_F \leq \frac{2^{3/2} \min\{\sqrt{K} \|(\alpha - xJ) \circ (I - N)\|_{op}, \|(\alpha - xJ) \circ (I - N)\|_F\}}{\xi_K - \xi_{K+1}} \quad (14)$$

for any  $x > 0$ .

Since  $| \{ (\alpha - xJ) \circ (I - N) \}_{i,j} |$  is upper-bounded hence is sub-Gaussian with bound parameter  $\sigma_e = \max_{i,j} \{ (1 + \epsilon) (D_i^{-1/2} - D_j^{-1/2})^2 A_{i,j} \}$ .

Using Theorem 1 of Duan, Michailidis and Ding 2020 (arXiv preprint:1910.02471), with probability  $1 - \delta_t$

$$\|\Psi_{1:K} - \phi_{1:K} R\|_F \leq \frac{2^{3/2} (\sqrt{K} p \sigma_e)}{\xi_K - \xi_{K+1}} t.$$

where  $\delta_t = \exp[-(t^2/64 - \log(5\sqrt{2}))p]$ . Taking  $t = 14$ , we have  $(t^2/64 - \log(5\sqrt{2})) > 1$ . Therefore, we have with probability at least  $1 - \exp(-p)$  {which is greater than  $1 - \exp(-n)$ }.

$$\|\Psi_{1:K} - \phi_{1:K} R\|_F \leq \frac{40\sqrt{K} p \sigma_e}{\xi_K - \xi_{K+1}}.$$

□

## S2.2 Proof of Theorem 2 and 3

Let the conditional probability associated with Gaussian leaf density  $f$  be  $\Pr\{B(y_1, M_n/2) | y_1\} = m_n$ , where  $B(y_1, M_n/2)$  stands for an open ball of radius  $M_n/2$  around  $y_1$ . If the true number of clusters is  $K = K_0$ , then  $m_n^{n-K-1}$  is the probability that the distances  $\{d_{\ell,n}^0\}_\ell$

in the minimum spanning tree under null are all below  $M$ . Specifically, let  $E_n = \{d_{\ell,n}^0 \leq M_n/2 : 1 \leq \ell \leq n - K - 1\}$ . Then  $\Pr(E_n) = m_n^{n-K-1}$ .

With  $x_i \sim N(0, \sigma^{0,n})$ , we have  $m_n = \Pr(\sum_{i=1}^p x_i^2 < \frac{M_n^2}{2^2 \sigma^{0,n}}) = 1 - \frac{\Gamma(p/2, \frac{M_n^2}{2^2 \sigma^{0,n}})}{\Gamma(p/2)}$ , where  $\Gamma(\cdot, \cdot)$  stand for the upper incomplete gamma function using cumulative distribution function of  $\chi^2$  distribution. Since  $p$  belongs to the set of natural numbers, we have  $\Gamma(p/2, x) < C_1 x^{p/2} e^{-x}$  except for  $p = 1.5$  and any  $x > 0$  with some constant  $C_1$  which depends on  $p$  (Pinelis, 2020). However, for large  $x$ , we have  $\Gamma(p/2, x) < C_1 x^{p/2} e^{-x}$  even for  $p = 1.5$ . We then have  $m_n > 1 - \frac{C_2}{\Gamma(p/2)} (\log n)^{p/2-1} e^{-\tilde{m}_0 \log n} = 1 - \frac{C_2}{\Gamma(p/2)} \frac{(\log n)^{p/2-1}}{n^{\tilde{m}_0}}$  where  $C_2 = C_1 (\tilde{m}_0)^{p/2-1}$ . Since  $\tilde{m}_0 > (p/2 + 2)$ , we have  $m_n^{n-K-1} > 1 - (n - K - 1) \frac{C_2}{\Gamma(p/2)} \frac{(\log n)^{p/2-1}}{n^{\tilde{m}_0}} \rightarrow 1$  as  $n \rightarrow \infty$  as  $\frac{\log n}{n}$  goes to 0. Hence  $\Pr(E_n) \rightarrow 1$ .

We further have,  $\sum_{n \geq K} [1 - \{1 - \frac{C_2}{\Gamma(p/2)} \frac{(\log n)^{p/2-1}}{n^{\tilde{m}_0}}\}^{n-K-1}] < \sum_n n \frac{C_2}{\Gamma(p/2)} \frac{(\log n)^{p/2-1}}{n^{\tilde{m}_0}}$ . Thus for  $\tilde{m}_0 > 2 + p/2$ , we have  $\sum_n [1 - \{1 - \frac{C_2}{\Gamma(p/2)} \frac{(\log n)^{p/2-1}}{n^{\tilde{m}_0}}\}^{n-K-1}] < \infty$ . Then, by the Borel-Cantelli Lemma, we also have almost sure convergence of this event.

We now show for  $y \in E_n$ , the ratio of the maximum posterior probability assigned to a “non-true” clustering arrangement to the posterior probability assigned to the “true” clustering arrangement converges to zero.

### Proof of Theorem 2

Note that for any  $\sigma$  and a given  $R$ , the posterior  $\Pi(\mathcal{T}_{\text{MST},R}, \sigma \mid y)$  is maximized at the  $\mathcal{T}$ , which is a combination of minimum spanning trees constructed within the regions  $R_k$ 's. Thus,

We have  $\frac{\Pi(R_0 \mid y)}{\Pi(\mathcal{T}_{\text{MST},R^0}, \sigma^{0,n} \mid y)} > 1$  as  $\Pi(R_0 \mid y) = \sum_{\mathcal{T}} \Pi(\mathcal{T}, R^0, \sigma^{0,n} \mid y)$ .

$$\begin{aligned} & \frac{\Pi(\mathcal{T}_{\text{MST},R}, \sigma^{0,n} \mid y)}{\Pi(\mathcal{T}_{\text{MST},R^0}, \sigma^{0,n} \mid y)} \\ & \leq \left(\frac{\epsilon_2}{\epsilon_1}\right)^K \exp\left(-\sum_{\ell=1}^{n-K_0-1} d_{\ell,n}^2 / (2\sigma^{0,n}) + \sum_{\ell=1}^{n-K-1} (d_{\ell,n}^0)^2 / (2\sigma^{0,n})\right), \end{aligned}$$

where  $\sum_{\ell=1}^{n-K-1} d_{\ell,n}^2$  is the total squared norm distance on the minimum spanning tree under the partition regions  $R$  excluding the edges with the root node and  $\sum_{\ell=1}^{n-K_0-1} (d_{\ell,n}^0)^2$  is the same under  $\mathcal{T}_{\text{MST},R^0}$ . The above is because based on the Prim's algorithm (Prim, 1957), the minimum spanning tree is equal to the result of sequential growing a tree starting from one node, each time by adding an edge (along with a node) with the shortest distance between one node in the existing tree and one of the remaining nodes not yet in the tree. Clearly, at each step, the edge choice is unaffected when changing distance from  $d$  to  $d^2$ ; therefore, the minimum spanning trees based on the sum of  $d_{\ell,n}^2$  and the sum of  $d_{\ell,n}$  are the same.

Since,  $\inf_{x \in R_i^0, y \in R_j^0} \|x - y\|_2 > M_n$ , for all  $i \neq j$ , for at least one  $\ell$ , we must have  $d_{\ell,n} > M$ . Due to the above result, with probability at least  $m_n^n$ , we have  $\sum_{\ell=1}^{n-K-1} (d_{\ell,n})^2 > \sum_{\ell=1}^{n-K-1} (d_{\ell,n}^0)^2 + M_n^2/4$ , which implies  $\frac{\Pi(\mathcal{T}_{\text{MST},R}, \sigma^{0,n} \mid y)}{\Pi(\mathcal{T}_{\text{MST},R^0}, \sigma^{0,n} \mid y)} < n^{-\tilde{m}_0}$ . And we further have that  $m_n^n \rightarrow 1$  as  $n \rightarrow 1$ .

### Proof of Theorem 3

First, we consider that the alternative partitioning has a lower number of clusters than

the null. Let that be  $K$ , which is less than  $K_0$ . Then we have

$$\frac{\Pi(\mathcal{T}_{\text{MST},R}, \sigma^{0,n} | y)}{\Pi(\mathcal{T}_{\text{MST},R^0}, \sigma^{0,n} | y)} \leq \lambda^{K-K_0} \frac{K_0!}{K!} \left( \frac{\epsilon_2}{\epsilon_1} \right)^K \frac{(\sigma^{0,n})^{(K_0-K)/2}}{\epsilon_1^{K_0-K}} \exp \left( - \sum_{\ell=1}^{n-K-1} d_{\ell,n}^2 / (2\sigma^{0,n}) + \sum_{\ell=1}^{n-K_0-1} (d_{\ell,n}^0)^2 / (2\sigma^{0,n}) \right),$$

We again must have  $\sum_{\ell=1}^{n-K-1} (d_{\ell,n})^2 > \sum_{\ell=1}^{n-K_0-1} (d_{\ell,n}^0)^2 + M_n^2/4$  with probability  $m_n^n \rightarrow 1$  as the alternative partitioning will have edges with length greater than  $M_n$ .

Next, we show the above when the alternative partitioning has a larger number of clusters than the null. Specifically, for  $K > K_0$ , we replace A3 and vary the conditions on  $r(y)$  with  $n$ .

Then we have

$$\frac{\Pi(\mathcal{T}_{\text{MST},R}, \sigma^{0,n} | y)}{\Pi(\mathcal{T}_{\text{MST},R^0}, \sigma^{0,n} | y)} \leq \lambda^{K-K_0} \frac{K_0!}{K_2!} \left( \frac{c_2}{c_1} \right)^K c_2^{K-K_0} (\sigma^{0,n})^{(K_0-K)/2} \times \exp \left( -(K-K_0)M_n^2 / (2\sigma^{0,n}) - \sum_{\ell=1}^{n-K-1} d_{\ell,n}^2 / (2\sigma^{0,n}) + \sum_{\ell=1}^{n-K_0-1} (d_{\ell,n}^0)^2 / (2\sigma^{0,n}) \right),$$

Again, for any  $K > K_0$ , the above ratio goes to zero as  $n \rightarrow \infty$  we have  $1/(\sigma^{0,n}n) \rightarrow 0$  with probability at least  $m_n^n \rightarrow 1$ .

### S3 Posterior consistency of the clustering

Here, we study the clustering consistency of our Bayesian methods when the number of clusters is known.

**Theorem S 1** *Under some assumptions outlined below, we have  $\Pi(R \neq R_0 | y) \rightarrow 0$  almost surely, unless  $R_i^0 \subseteq R_{\xi(i)}$  for some permutation map  $\xi(\cdot)$  when number of clusters is known.*

The total number of possible clusters with  $n$  data points and  $K$  clusters is  $\binom{n-1}{K-1}$ , which is of order  $n^K$ . To show clustering consistency, we require the following assumption,

- (S1, Diminishing scale and minimum separation) We let  $\sigma^{0,n} = C'(1/n \log^{1+\iota} n)$  for some  $\iota > 0$  and  $C' > 0$  and  $\inf_{x \in R_k^0, y \in R_{k'}^0} \|x - y\|_2 > M_n$ , for all  $k \neq k'$  with some positive constant  $M_n > 0$  such that  $M_n^2 / \sigma^{0,n} = 8\tilde{m}_0 n \log(n)$  for all  $(i, j)$  and is known for some constant  $\tilde{m}_0 > p/2 + 2$ .

In the above assumption, the main requirement is  $M_n^2 / \sigma^{0,n} = 8\tilde{m}_0 n \log(n)$  which is achieved by allowing the scale to decay faster than Assumption A1. Alternatively, one may increase  $M_n$  instead of reducing  $\sigma^{0,n}$ . However, from a practical point of view, one would expect  $M_n$  to be a non-increasing function of  $n$ .

$$\frac{\Pi(R | y)}{\Pi(R_0 | y)} = \frac{\frac{\Pi(R|y)}{\Pi(\mathcal{T}_{\text{MST},R,\sigma^{0,n}|y})}}{\frac{\Pi(R_0|y)}{\Pi(\mathcal{T}_{\text{MST},R^0,\sigma^{0,n}|y})}} \frac{\Pi(\mathcal{T}_{\text{MST},R,\sigma^{0,n}} | y)}{\Pi(\mathcal{T}_{\text{MST},R^0,\sigma^{0,n}} | y)},$$

We have  $\frac{\Pi(R_0|y)}{\Pi(\mathcal{T}_{\text{MST},R^0,\sigma^{0,n}|y})} > 1$  and  $\frac{\Pi(R|y)}{\Pi(\mathcal{T}_{\text{MST},R,\sigma^{0,n}|y})} < n^{n-2}$  (the total number of possible spanning trees with  $n$  points) hence  $\frac{\Pi(R|y)}{\Pi(R_0|y)} \lesssim n^{n-2} \frac{\Pi(\mathcal{T}_{\text{MST},R,\sigma^{0,n}} | y)}{\Pi(\mathcal{T}_{\text{MST},R^0,\sigma^{0,n}} | y)}$

When the number of clusters is known,

$$\frac{1 - \Pi(R^0 | y)}{\Pi(R^0 | y)} = \sum_{R \neq R^0} \frac{\Pi(R | y)}{\Pi(R^0 | y)} \lesssim \exp((n + K - 2) \log n) \frac{\Pi(\mathcal{T}_{\text{MST},R,\sigma^{0,n}} | y)}{\Pi(\mathcal{T}_{\text{MST},R^0,\sigma^{0,n}} | y)}$$

And applying the steps from our previous section, we have  $\frac{1 - \Pi(R^0|y)}{\Pi(R^0|y)} < \exp(-n \log n)$ , goes to zero and thus completes the proof.

## S4 Additional Numerical Experiments

### S4.1 Uncertainty Quantification on Clustering Data from a Mixture Model

We now present some uncertainty quantification results, for clustering data that are from a mixture model. We experiment with  $n = 400$  data points in  $\mathbb{R}^2$  generated from a two-component mixture distribution:

$$y_i \sim 0.5\mathcal{K}(\cdot | \mu_1) + 0.5\mathcal{K}(\cdot | \mu_2),$$

for  $i = 1, \dots, n$ , with  $\mu_1 = (0, 0)$  and  $\mu_2 = (b, b)$  two location parameters. We experiment with two settings, with  $\mathcal{K}$  as (i) independent bivariate Gaussian distribution  $N(\mu_k, I_2)$ , (ii) independent bivariate  $t$  distribution with 5 degrees of freedom  $t_5(\mu_k)$ .

When fitting models, we consider the unknown  $K$  scenario, and use the distribution  $\Pi(\mathcal{T}) \propto \lambda^K$  for the Bayesian forest model, with  $\lambda = 0.5$ . For comparison, we use the Dirichlet process Gaussian mixture model (DP-GMM) with a Gamma(2, 20) hyper-prior on the concentration parameter (with prior mean 0.1). We use the “dirichletprocess” package in R (Ross and Markwick, 2018) for estimating the posterior distribution from DPMM. Notice that our two choices of  $\mathcal{K}$  above correspond to fitting a Dirichlet process mixture with correctly specified components and one with misspecified components, respectively.

To estimate the posterior, for each model, we ran the MCMC algorithm for 1,000 iterations and discarded the first 500 iterations. We calculated the posterior co-assignment probability matrix  $\Pr(c_i = c_j | y)$ , and the posterior number of clusters  $\Pr(K | y)$ .

When the data are from the Gaussian mixture (Figure S.5), both the DP-GMM and the forest model lead to satisfactory performances, with the mode of  $\Pr(K | y)$  equal/close to the ground truth at  $K = 2$ . It is interesting to note that there is a proportion of the posterior sample from the forest model corresponds to  $K = 1$ . This is likely due to less parametric assumption imposed on the shape of the clusters, compared to the DP-GMM. Nevertheless, the posterior mode of the forest model correctly falls on  $K = 2$ .

On the other hand, when the data are from the  $t_5$  mixture (Figure S.6), we find the DP-GMM always show an over-estimation problem. Such issues are due to the misspecification in the component distribution, and Cai et al. (2021) have shown that switching to a finite Gaussian mixture with a prior on  $K$  does not solve the problem. In comparison, the clustering of the forest model shows much less sensitivity to model specification.



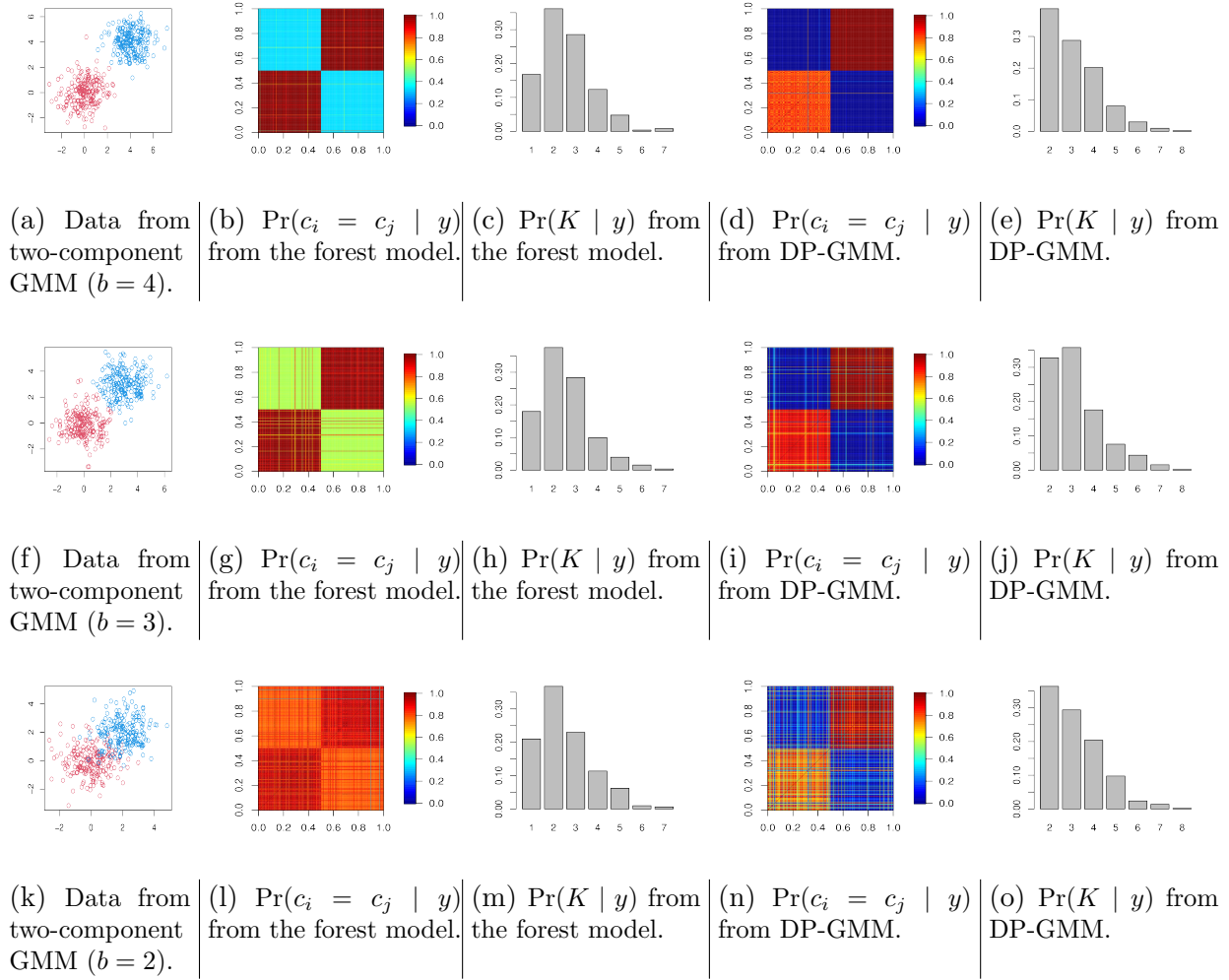


Figure S.4: Uncertainty quantification in clustering data generated from a two-component Gaussian mixture model.

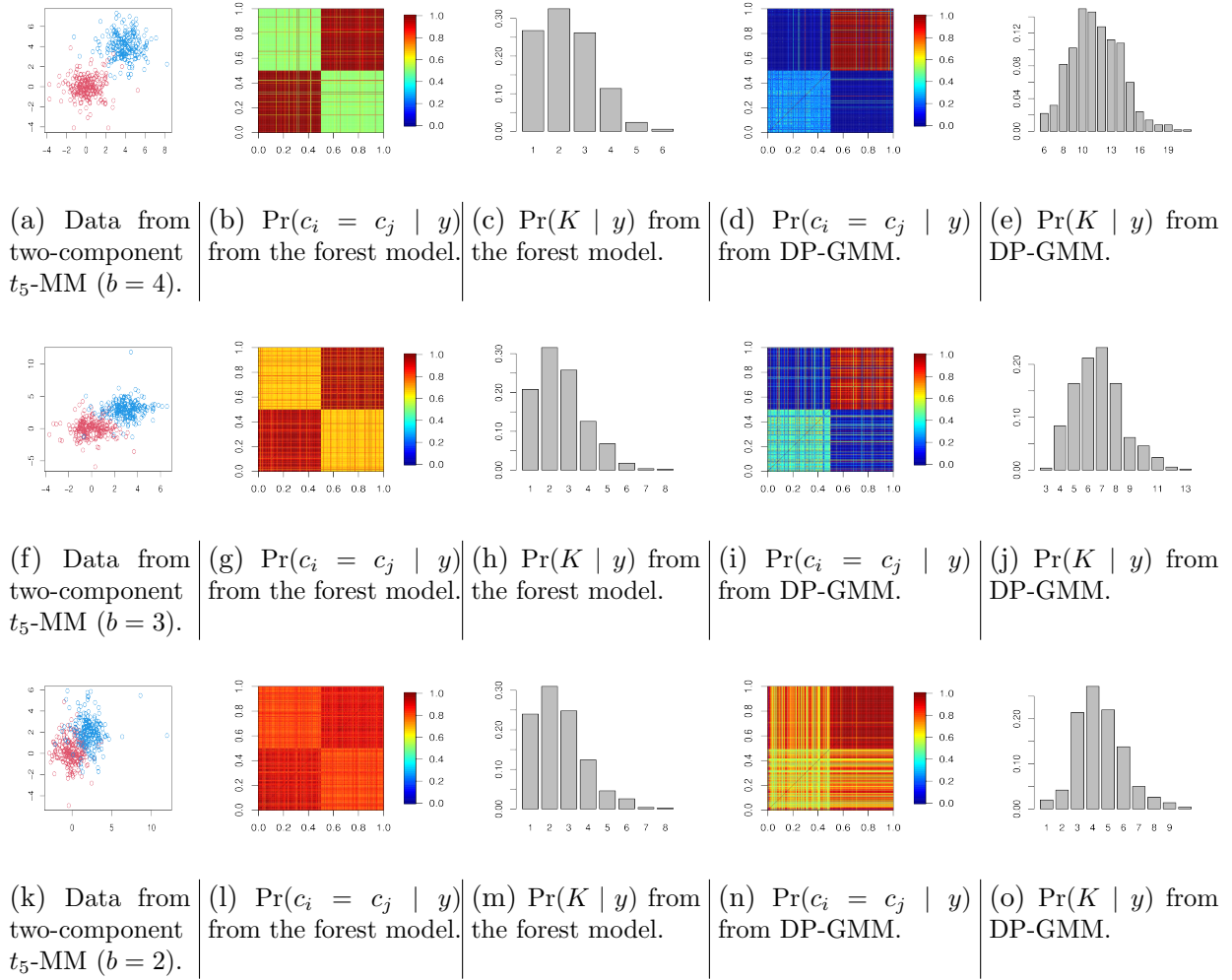


Figure S.5: Uncertainty quantification in clustering data generated from a two-component  $t_5$  mixture model.

## S4.2 Additional Experiments on Clustering Near-Manifold Data

We conduct additional simulations on clustering near-manifold data. The results are shown in Figure S.7.

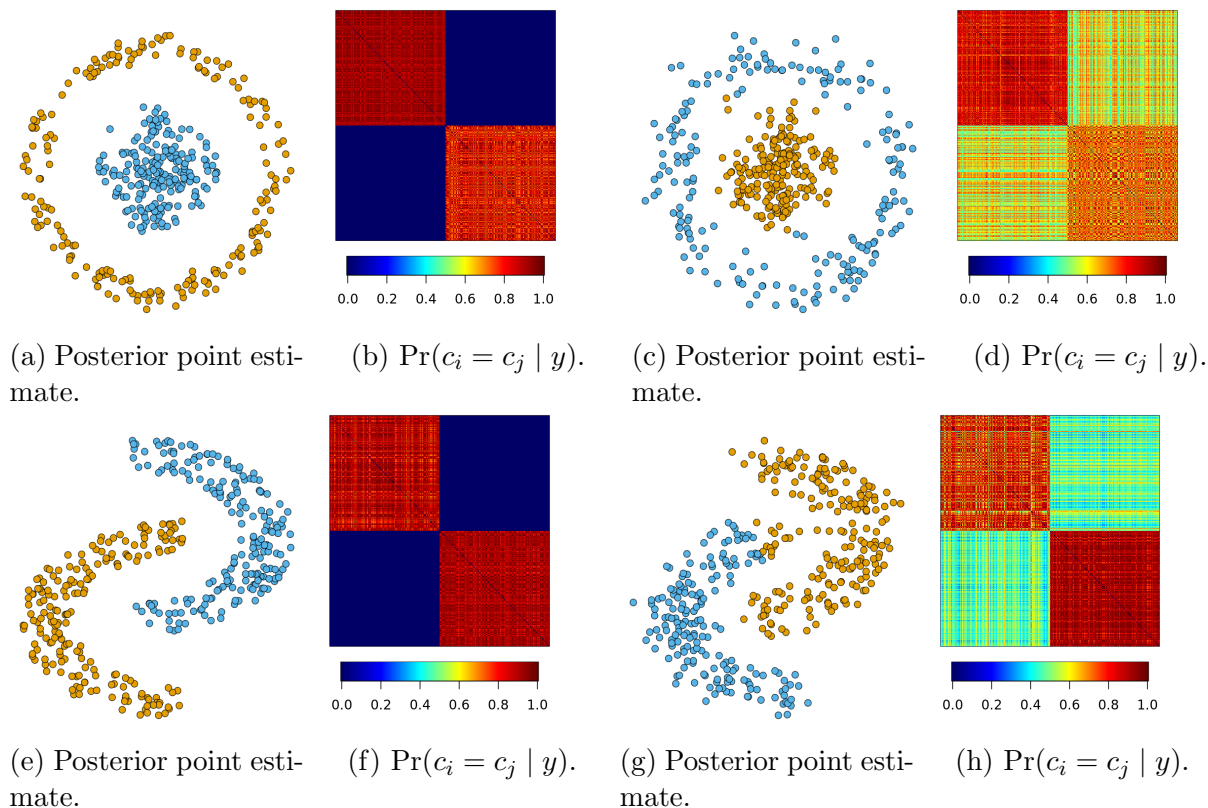


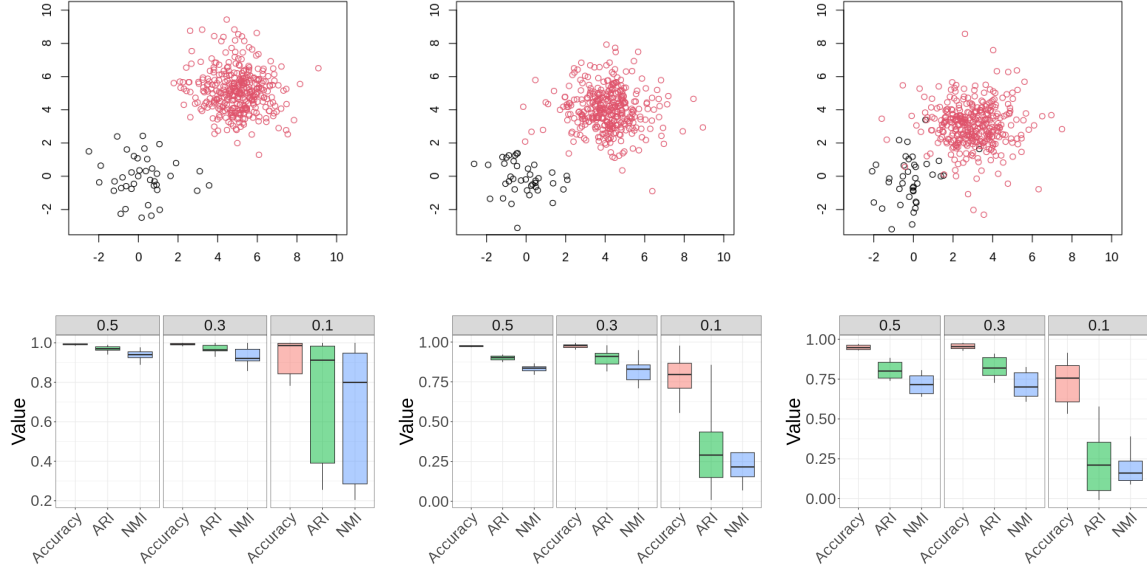
Figure S.6: Clustering data generated near manifolds.

### S4.3 Additional Simulations on Uncertainty and Clustering Accuracy

We now compare the uncertainty and clustering accuracy. We consider three possible scenarios as different sources of uncertainties: increasingly imbalanced cluster sizes, an increasing number of clusters, and an increasing number of noisy points between clusters. In addition, we gradually reduce the separation between clusters, so that the uncertainty can increase as well.

When measuring the clustering accuracy of the point estimate, we calculate the adjusted Rand index (ARI), normalized mutual information (NMI), as well as the clustering accuracy rate (the match rate between the point estimate of  $\hat{c}_i$  and each ground-truth label, minimized over all possible label switchings in  $\hat{c}_i$ ). We run 10 times of experiments under each combination of values, and show the boxplots.

For the first scenario, we generate  $n = 400$  data points from a two-component independent bivariate  $t$  distribution with 5 degrees of freedom,  $y_i \sim \tilde{w}_1 t_5(\cdot | [0, 0]) + (1 - \tilde{w}_1) t_5(\cdot | [\tilde{b}, \tilde{b}])$ . We experiment with different values of  $\tilde{w}_1 \in \{0.5, 0.3, 0.1\}$  to have different degrees of cluster size imbalance, as well as different values of  $\tilde{b} \in \{5, 4, 3\}$  to have different degrees of separation between cluster centers. The results are shown in Figure 12.



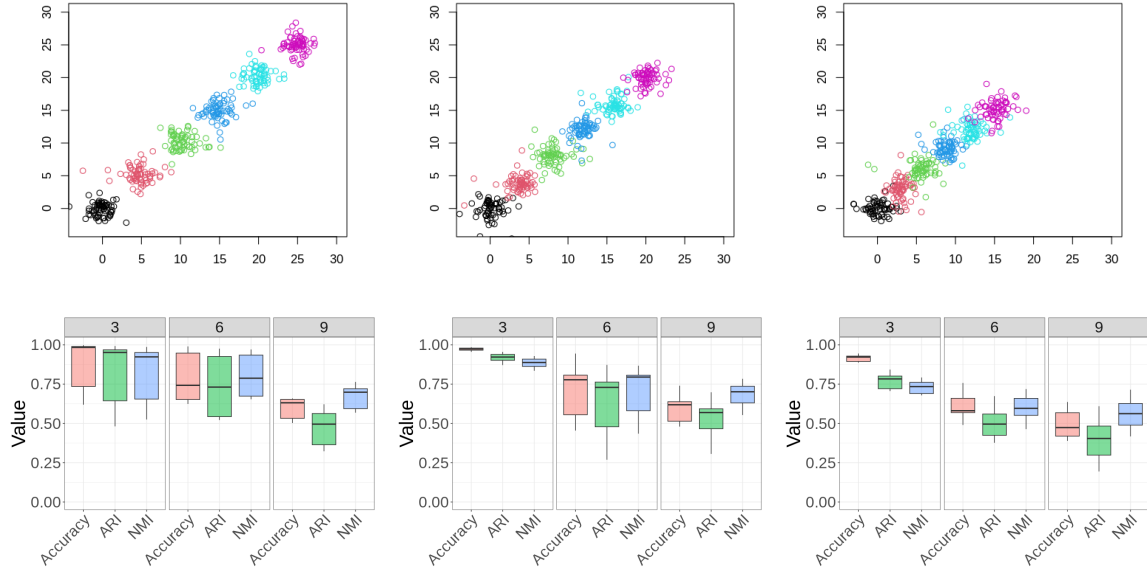
(a) Two clusters of imbalanced sizes with two means separated by vector  $[5, 5]$  (above). The experiments are repeated with the proportion of Cluster 1 size taken from  $\{0.5, 0.3, 0.1\}$ , and the clustering accuracy measures are shown below.

(b) Two clusters of imbalanced sizes with two means separated by vector  $[4, 4]$  (above). The experiments are repeated with the proportion of Cluster 1 size taken from  $\{0.5, 0.3, 0.1\}$ , and the clustering accuracy measures are shown below.

(c) Two clusters of imbalanced sizes with two means separated by vector  $[3, 3]$  (above). The experiments are repeated with the proportion of Cluster 1 size taken from  $\{0.5, 0.3, 0.1\}$ , and the clustering accuracy measures are shown below.

Figure 12: Clustering accuracy decreases as the cluster sizes become more imbalanced. The adjusted Rand index (ARI), normalized mutual information (NMI), and the clustering accuracy rate (Accuracy, the match rate between  $\hat{c}_i$  and the ground truth, minimized over all possible label switchings in  $\hat{c}_i$ ) are shown.

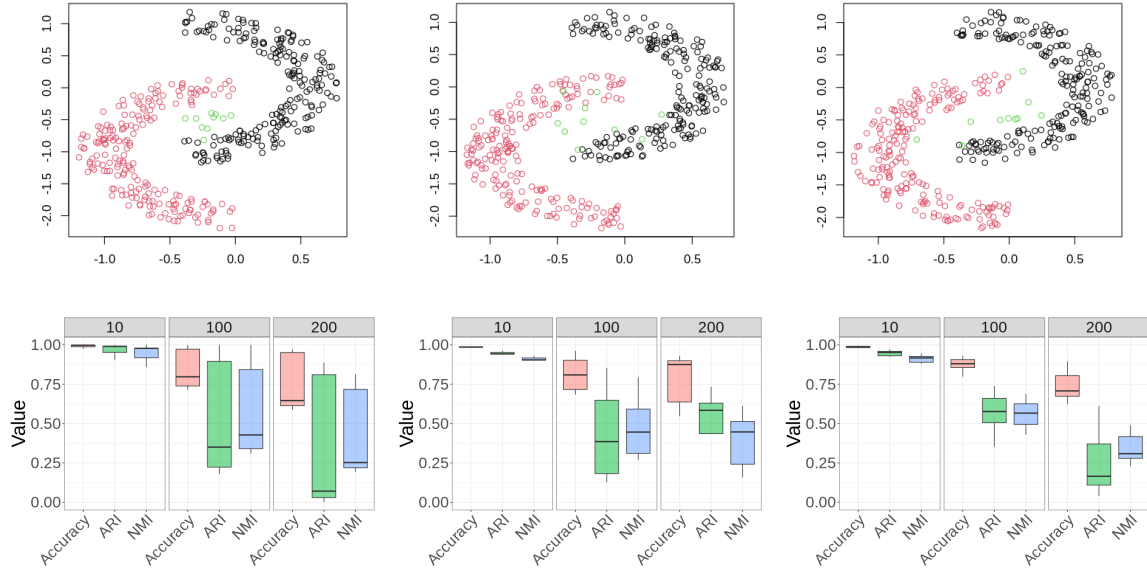
For the second scenario, we generate  $n = 400$  data points from a  $\tilde{K}$ -component bivariate  $t$  distribution with 5 degrees of freedom,  $y_i \sim \sum_{k=1}^{\tilde{K}} (1/\tilde{K}) t_5(\cdot \mid [b_k, b_k])$ . We experiment with different values of  $\tilde{K} \in \{3, 6, 9\}$  to have different numbers of clusters, as well as different values of  $b_k = 3(k-1)$ ,  $4(k-1)$  or  $5(k-1)$  to have different degrees of separation between cluster centers. The results are shown in Figure 13.



(a) Increasing number of clusters. (b) Increasing number of clusters. (c) Increasing number of clusters.

Figure 13: Clustering accuracy decreases as the number of clusters increases. The adjusted Rand index (ARI), normalized mutual information (NMI) and the clustering accuracy rate (Accuracy, the match rate between  $\hat{c}_i$  and the ground-truth, minimized over all possible label switchings in  $\hat{c}_i$ ) are shown.

For the third scenario, we first generate  $n = 400$  data points near the two moon manifolds that are well separated from one another, then we add  $m$  number of points generated from Gaussian distribution with variance  $\tilde{\gamma}^2$ , and its center placed between the two manifolds. We experiment with different values of  $m \in \{10, 100, 200\}$ , so that the clusters would appear somewhat connected to each other as  $m$  increases; we also vary  $\tilde{\gamma}^2 \in \{0.1^2, 0.2^2, 0.3^2\}$  to have different levels of noise. The results are shown in Figure 14.

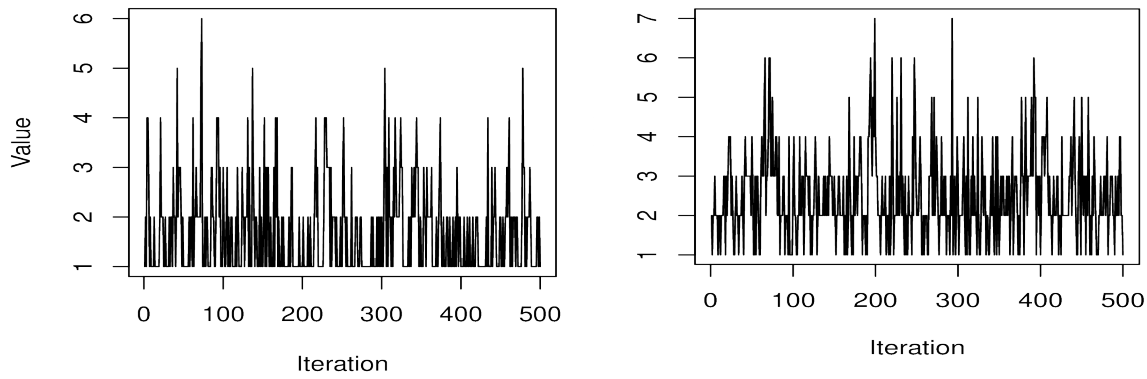


(a) Noisy points (green, with variance  $0.1^2$ ) between clusters (above). The clustering accuracy measures are collected (below) with the number of noisy points taken from  $\{10, 100, 200\}$ .  
 (b) Noisy points (green, with variance  $0.2^2$ ) between clusters (above). The clustering accuracy measures are collected (below) with the number of noisy points taken from  $\{10, 100, 200\}$ .  
 (c) Noisy points (green, with variance  $0.3^2$ ) between clusters (above). The clustering accuracy measures are collected (below) with the number of noisy points taken from  $\{10, 100, 200\}$ .

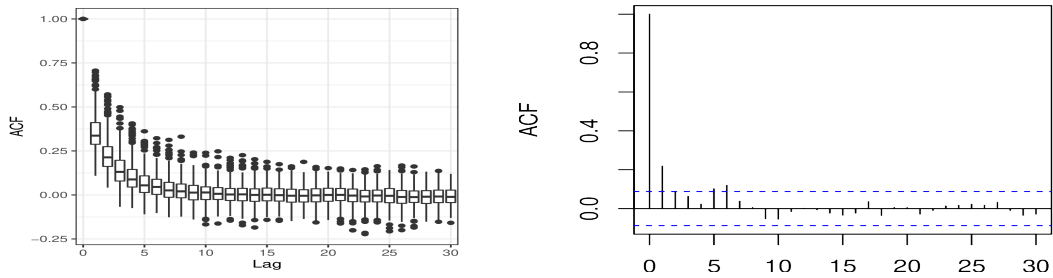
Figure 14: Clustering accuracy decreases as the number of noisy points between clusters increases. The adjusted Rand index (ARI), normalized mutual information (NMI), and the clustering accuracy rate (Accuracy, the match rate between  $\hat{c}_i$  and the ground truth, minimized over all possible label switchings in  $\hat{c}_i$ ) are shown.

#### S4.4 Diagnostic plots for Markov chain Monte Carlo

The MCMC algorithm that we describe in the main text shows a fast mixing of Markov chains. To illustrate this, we use the Markov chain collected from the experiment related to Figure S.6(k), and calculate the autocorrelations in (i) the degrees for each node in the forest  $D_{i,i}$ 's, and (ii) the number of clusters  $K$ . We plot the results in Figure S.8.



(a) Traceplot of one degree in the forest  $D_{1,1}$ . (b) Traceplot of the number of clusters  $K$ .



(c) Boxplot of the autocorrelations for  $D_{i,i}$ 's. (d) Autocorrelation for the number of clusters  $K$ .

Figure S.10: Traceplots and autocorrelation plots show fast mixing of the MCMC algorithm.

To demonstrate the high efficiency of updating  $\mathcal{T}$  in a block via the random-walk covering algorithm (Broder, 1989; Aldous, 1990; Mosbah and Saheb, 1999), we plot the sampled  $\mathcal{T}$  at three contiguous iterations (after burn-ins) in Figure S.9. The forest shows a rapid change from iteration to iteration — indeed, the proportion of edge changes (the number of edges  $\{(i, j) : (i, j) \in \mathcal{T}_{[t]}, (i, j) \notin \mathcal{T}_{[t+1]}\}$  divided by the total number of edges) is around 50% at each iteration.

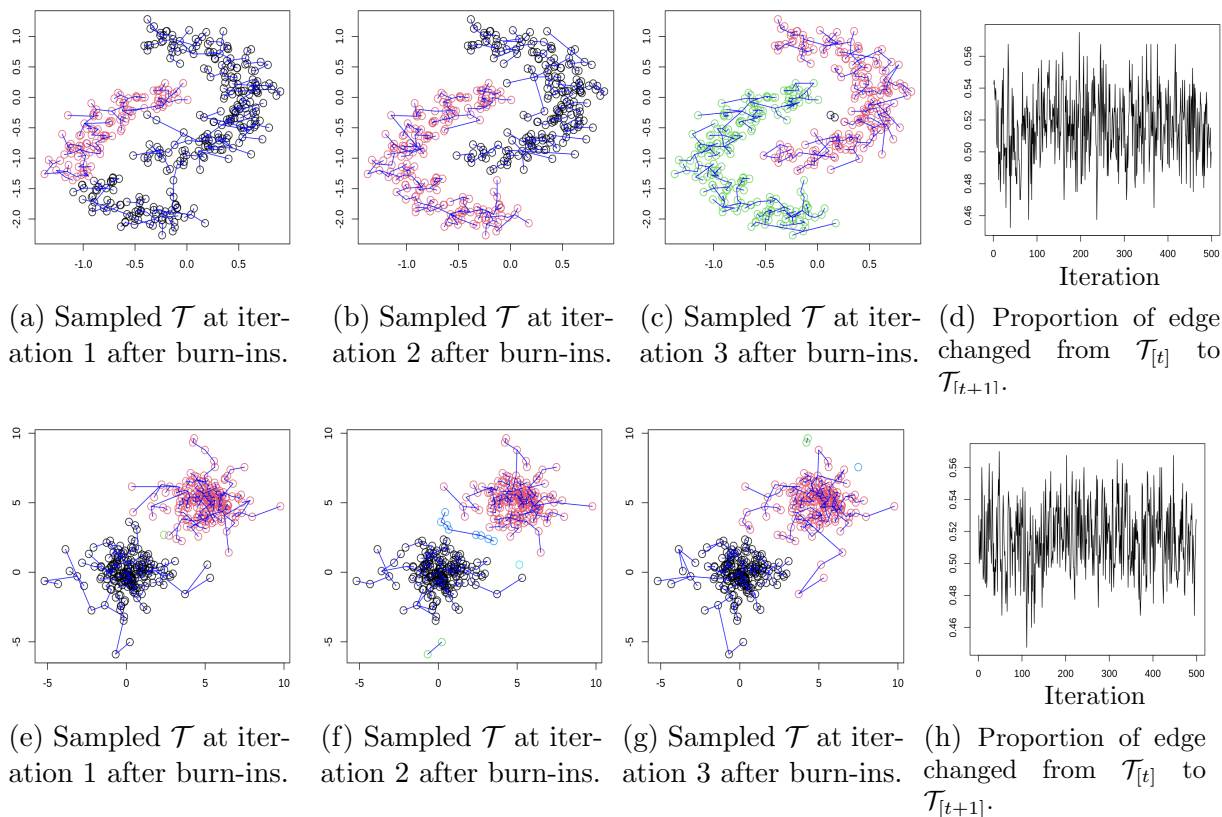
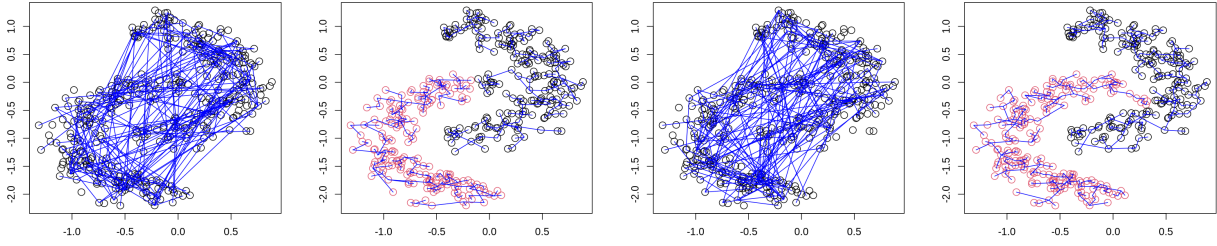


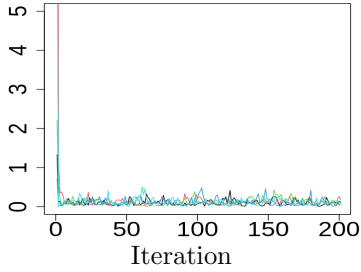
Figure S.11: The forest  $\mathcal{T}$  changes rapidly from one iteration to another: Panels a-c plot the forests (blue) at three contiguous iterations, and Panel d shows the proportion of edge changes in each iteration, as measured by the number of edges  $\{(i, j) : (i, j) \in \mathcal{T}_{[t]}, (i, j) \notin \mathcal{T}_{[t+1]}\}$  divided by the total number of edges. Panels e-h show the results from another experiment. In both cases, the forest  $\mathcal{T}$  has about 50% of edges changed from one iteration to the next.

Further, we assess the convergence by randomly initializing  $(\mathcal{T}_{[0]}, \theta_{[0]})$  at 5 different start points, and run 5 separate Markov chains. Specifically, for the elements  $\tilde{\sigma}_i$  and  $\gamma$  in  $\theta_{[0]}$ , we initialize them randomly from Inverse-Gamma(0.5, 0.5), then we draw  $\mathcal{T}_{[0]} \sim \Pi(\mathcal{T} \mid \theta_{[0]}, y)$ . Figure S.10 shows two randomly initialized  $\mathcal{T}$ 's. The traceplots of the parameters show the convergence of 5 Markov chains, and we calculate the Gelman–Rubin statistics (potential scale reduction factor, Gelman and Rubin (1992)) and find all of them smaller than 1.1, which indicates convergence.

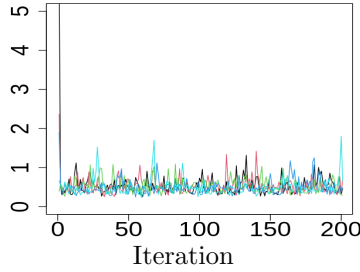




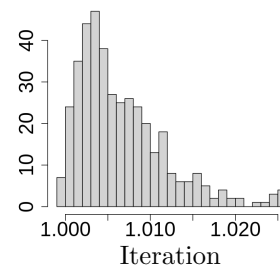
(a) Randomly initialized  $\mathcal{T}$  in Chain 1. (b) One sampled  $\mathcal{T}$  in Chain 1 after burn-ins. (c) Randomly initialized  $\mathcal{T}$  in Chain 2. (d) One sampled  $\mathcal{T}$  in Chain 2 after burn-ins.



(e) Traceplot for the parameter  $\tilde{\sigma}_1$  from 5 chains.



(f) Traceplot for the parameter  $\gamma$  from 5 chains.



(g) Histogram of the Gelman-Rubin statistics for all  $\tilde{\sigma}_i$ 's and  $\gamma$ .

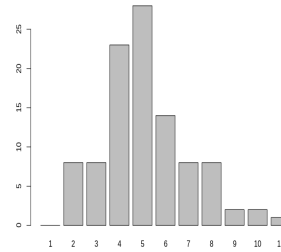
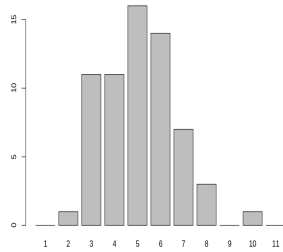
Figure S.12: The convergence of five randomly initialized Markov chains.

## S4.5 Additional Details on the Multi-view Clustering in the Alzheimer’s Disease Study



(a) The average  $\Pr(c_i = c_j | y)$  for the ROIs in the healthy group.

(b) The average  $\Pr(c_i = c_j | y)$  for the ROIs in the diseased group.



(c) Frequency plot of the number of clusters of ROIs for each subject in the healthy group.

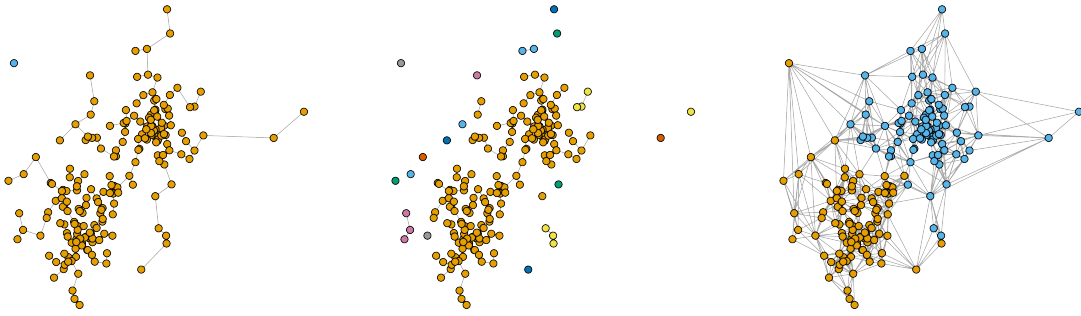
(d) Frequency plot of the number of clusters for each subject in the diseased group.

Figure S.13: Clustering estimates for the healthy and diseased group.

## S4.6 Comparison with Minimum Spanning Tree-based Cut

Since our Bayesian forest model uses spanning trees, it is natural to compare with the clustering algorithm based on cutting the minimum spanning tree (MST). To formalize, the minimum spanning tree-based cut (MST-Cut) algorithm first finds the MST:  $\hat{T} = \arg \min_{T \in \mathbb{T}_n} \sum_{(i,j) \in T} \|y_i - y_j\|$ , where  $\mathbb{T}_n$  denotes all spanning trees that connect  $n$  nodes, with  $\|y_i - y_j\|$  as some distance between the two points. Then, one removes the longest  $(K - 1)$  edges (with length defined as  $\|y_i - y_j\|$ ) to create  $K$  clusters. This algorithm is shown to be equivalent to the single-linkage clustering algorithm (Hartigan, 1981).

As we could imagine, such MST-Cut algorithms work well when clusters are well separated. In that case, those clusters will more likely be connected by the longest few edges. However, such algorithms will suffer sensitivity issues, when any one or more of the following happens: 1) when clusters are close to each other; 2) when a few isolated points are lying between two clusters; 3) when one or more clusters are from a heavy-tailed distribution, with a few points away from the bulk of the cluster. As a result, the longest edges in the MST may not be ideal for partitioning data.



(a) Partitioning the data by cutting the longest edge in the minimum spanning tree. (b) Partitioning the data by cutting the top 10% longest edges in the minimum spanning tree. (c) Partitioning the data using the Bayesian spanning forest model.

Figure 19: Comparing point estimates from the minimum spanning tree-based cut (MST-Cut) algorithms and the Bayesian spanning forest model.

To illustrate this problem, we use a simulation with data from a two-component  $t$ -distribution in  $\mathbb{R}^2$  with 3 degrees of freedom. One component has the mean  $(0,0)$  and the other has  $(4,4)$ , and both have the scale parameter equal to  $I_2$ . And we generate  $n = 200$  data points. As shown in Figure 19(a), due to the heavy tail and closeness of the two clusters, cutting the longest edge in the MST (using Euclidean distances) yields a trivial and sub-optimal partition. Further, cutting the top 10% longest edges still does not produce the desired result (Panel b).

Fundamentally, the reason is that relying on the minimum spanning tree (that is, one tree) leads to an underestimation of the graph uncertainty. Different from the MST-Cut algorithms, the Bayesian forest model effectively uses the marginal distribution (3) incorporating the multiplicity of those likely trees (with edges shown in Panel c). As the result, it leads to better performance than the MST-Cut algorithm.

### S4.7 Empirical Evidence for the Fast Convergence of Eigenvectors

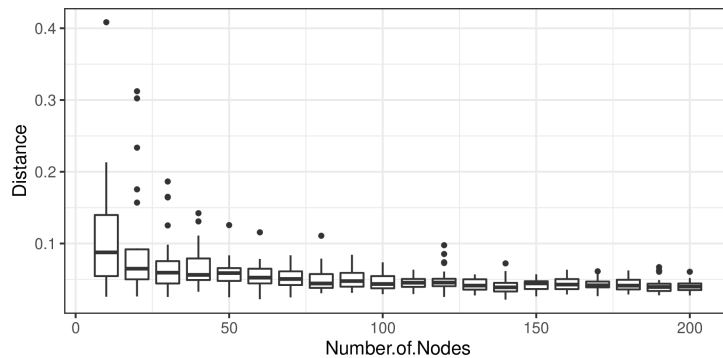


Figure S.15: The difference between eigenvectors converges to zero rapidly as  $n$  increases.

We now use simulations to illustrate the closeness between the  $K$  leading eigenvectors of the marginal connecting probability matrix  $M$  and the ones of the normalized Laplacian  $N$ . It is important to clarify that such closeness does not depend on how the data are generated. Therefore, for simplicity, we generate  $y_i$  from a simple three-component Gaussian mixture in  $\mathbb{R}^2$  with means in  $(0, 0)$ ,  $(2, 2)$ ,  $(4, 4)$  and all variances equal to  $I_2$ , then we fit our forest model, and estimate  $\sigma_{i,j}$ 's using posterior mean. Based on the posterior mean of  $\sigma_{i,j}$ , we compute  $M$  and  $N$ , and then compute distances between their leading eigenvectors  $\min_{R:RR'=I_K} \|\Psi_{1:K} - \Phi_{1:K}R\|$ . We conduct such experiments under different sample sizes  $n$  ranging from 10 to 200; for each  $n$ , we repeat experiments for 30 times. As our theory requires a spectral gap  $\xi_K - \xi_{K+1}$  not too close to zero, we choose to compare the top  $K = 5$  eigenvectors. As shown in the boxplot of Figure S.4, the distance between two sets of eigenvectors quickly drops to near zero, for  $n \geq 50$ .

## S5 Alternative Model for the Scale Parameters

As an alternative to specifying a prior on the scale parameter  $\tilde{\sigma}_i$  in the leaf density, the heuristic of setting  $\tilde{\sigma}_i$  to a low order statistic of  $\{\|y_i - y_j\|_2\}_{j=1}^n$  is shown to enjoy a good empirical performance in spectral clustering (Zelnik-Manor and Perona, 2005). In this section, we extend this heuristic to a formal model-based solution.

To start, we first relate the small distances to the  $\tilde{k}$ -nearest neighbor density estimator. Loftsgaarden and Quesenberry (1965) show that for  $y_1, \dots, y_n$  iid from a distribution with probability density  $f$ , with a growing  $\tilde{k} \rightarrow \infty$ ,  $\tilde{k}/n \rightarrow 0$  as  $n$  increase, if  $f$  is continuous at  $y_i$ , the  $\tilde{k}$ -nearest neighbor density estimator  $f_n(y_i) = \tilde{k}/[nV_{\tilde{k}}(y_i)]$  is consistent for estimating  $f(y_i)$ , where  $V_{\tilde{k}}(y_i)$  is the volume of the ball centered at  $y_i$  and with radius equal to the distance to the  $\tilde{k}$ -th nearest neighbor, denoted by  $d_i^{(\tilde{k})}$  from now on.

Although we no longer consider data as iid,  $d_i^{(\tilde{k})}$  is still informative on how dense the data points are near  $y_i$ . Therefore, to bring information from  $d_i^{(\tilde{k})}$  into the spanning forest model-based clustering, we consider a generative model that simultaneously depends on a spanning forest (with  $K$  component trees) and a  $\tilde{k}$ -nearest neighbor graph  $\tilde{G}_{nn}$ . We can use a likelihood

$$\begin{aligned} \mathcal{L}(y; \tilde{G}_{nn}, \mathcal{T}, \theta) \propto & \left\{ \prod_{i=1}^n \frac{(\tilde{\sigma}_i)^{\alpha_\sigma}}{\Gamma(\alpha_\sigma)} \left[ \frac{d_i^{(\tilde{k})}}{\sqrt{p}} \right]^{-\alpha_\sigma - 1} \exp \left[ -\frac{\tilde{\sigma}_i}{d_i^{(\tilde{k})}/\sqrt{p}} \right] \right\} \\ & \cdot \prod_{k=1}^K \left\{ r(y_{k^*}; \theta) \prod_{(i,j) \in T_k} (2\pi\sigma_{i,j})^{-p/2} \exp \left( -\frac{\|y_i - y_j\|_2^2}{2\tilde{\sigma}_i\tilde{\sigma}_j} \right) \right\}. \end{aligned}$$

And one can verify that each term on the right-hand side is integrable in  $y_i$ , even if  $d_i^{(\tilde{k})} = \|y_i - y_j\|_2$  happened (that is, when  $(i, j) \in T_k$  and  $j$  happened to be the  $\tilde{k}$ -nearest neighbor of  $i$ ); therefore, the right-hand side forms a proper likelihood. We choose the inverse-gamma distribution for each  $d_i^{(\tilde{k})}/\sqrt{p}$ , as it leads to an equivalent  $\text{Gamma}(\alpha_\sigma + 1, d_i^{(\tilde{k})}/\sqrt{p})$  distribution for  $\tilde{\sigma}_i$  that produces a shrinkage effect on  $\tilde{\sigma}_i$  (Brown and Griffin, 2010), and it enjoys closed-form Gibbs sampling update via the generalized inverse gaussian distribution. We test the above model using  $\tilde{k} = \lceil n^{1/10} \rceil$ , and  $\alpha_\sigma = 1$  on all the examples presented in

the article, and the results are quite similar to the ones shown in the main text. We provide the implementation in the R source code.

## **S6 Software Source Code**

The software source code for this paper can be found under [this link](#) on github.